NTNU

Norwegian University of
Science and Technology

Finite Element Analysis of Suction Bucket Foundations in Sand Subjected to Cyclic Loading

Ingerid Elisabeth Rolstad Jahren

Civil and Environmental Engineering
Submission date: June 2018
Supervisor: Hans Petter Jostad, IBM

Norwegian University of Science and Technology
Department of Civil and Environmental Engineering

Preface

This is a master thesis written in the spring of 2018 as the final part of my M.Sc. degree in Civil and Environmental Engineering at the Norwegian University of Science and Technology (NTNU) in Trondheim. The thesis is a part of the master's programme in Geotechnical Engineering at the department of Civil and Environmental Engineering. The thesis has been carried out in a cooperation with the Norwegian Geotechnical Institute (NGI), which also proposed the thesis.

Trondheim, 2018-06-10

Ingerid Rolstad Jahren

Acknowledgement

I would like to express my gratitude to my academic supervisor Adjunct Prof. Hans Petter Jostad, NGI, who provided great insight and expertise throughout the thesis work. His interest and enthusiasm for the topic in addition to great knowledge is truly inspiring.

I also thank members of the staff at the Geotechnical Division at NTNU for kindly sharing their wisdom during my years as a student at NTNU.

Finally, thank you to all my fellow students for valuable discussions and support.

I.R.J.

Abstract

A suction bucket or suction caisson is a foundation concept for supporting offshore installations. The practical experience related to this concept is mainly based on applications in the oil and gas industry. Observations show significant difference in response for wind turbines compared to more traditional installations offshore. The lightweight structure of a wind turbine makes the caisson susceptible to cyclic loading due to metocean conditions. As this foundation concept is being increasingly considered for offshore wind turbines, a proper understanding of its behaviour is important for a functional and effective design of suction caissons for this purpose.

A series of centrifuge experiments have been performed at the University of Western Australia to investigate the response of a suction caisson in dense Baskarp sand. The experiments aim to represent the load conditions of a caisson supporting an offshore wind turbine in the North Sea. Raw data from the centrifuge experiments have in this thesis been analysed focusing on the cyclic response, and the work demonstrates a significant difference in response for compression and tension loading. The permeability of the soil is also found to be decisive for the caisson response.

A model of the centrifuge experiment in prototype scale is in this study recreated in the finite element software PLAXIS. Model parameters are based on tests on similar sand available at NGI, due to limitations of sand specific cyclic laboratory tests related to the centrifuge experiments. Arbitrary sets of parameters, representing sands of different densities, are also considered. Loads identical to those of the centrifuge experiments is applied to the simulations.

Results from the simulations differ from the centrifuge experiments. Displacements are in general underestimated and total stress and pore pressure are overestimated. Several reasons to the differences are discussed in the thesis, and these are assumed to be related to calibration of the permeability, loosening of the sand due to installation, lack of fully contact between caisson lid and soil in addition to air bubbles in the pore fluid. The differences emphasise the challenge of capturing all features of the complex caisson response in a simplified model.

Sammendrag

Bøttefundament eller sugeanker er et fundamenteringskonsept for offshore-installasjoner. Den praktiske erfaringen tilknyttet dette konseptet er i hovedsak basert på anvendelser i olje- og gassektoren. Undersøkelser viser en betydelig forskjell i oppførsel for vindturbiner sammenlignet med mer tradisjonelle installasjoner offshore. Den lette vindmøllekonstruksjonen gjør bøttefundamentet sårbart for syklisk last fra vind, bølger og havstrømmer. Dette fundamenteringskonseptet blir i økende grad vurdert for offshore vindmøller, og en god forståelse av dets oppførsel er viktig for en funksjonell og effektiv utforming av bøttefundament til dette formålet.

En rekke sentrifugeforsøk er utført ved University of Western Australia for å analysere oppførselen til et bøttefundamet plassert i tettpakket Baskarp-sand. Forsøkene streber etter å gjenskape lastforholdene for en offshore vindmølle plassert på toppen av et fundament i Nordsjøen. Rådata fra forsøkene er i denne avhandling analysert med fokus på syklisk respons, og arbeidet viser en betydelig forskjell i respons avhengig av strekk- og trykkbelastning. Resultater fra forsøkene viser også at permeabiliteten i sanden er avgjørende for oppførselen til bøttefundamentet.

En modell av sentrifugeforsøkene i prototypeskala er i forbindelse med dette studiet laget i finite element-programmet PLAXIS. Sandparametre er basert på tester av tilsvarende materiale tilgjengelig ved NGI, da slike type tester ikke er gjennomført i forbindelse med sentrifugeforsøkene. Et sett av materialer med ulike densitet er også undersøkt. Lasttilfeller identisk til sentrifugeforsøkene er benyttet i simuleringene.

Resultater fra simuleringene viser avvik fra sentrifugetestene. Forskyvningen er generelt underestimert og total- og poretrykk er overestimert. Oppgaven diskuterer mulige årsaker til avviket, og disse er antatt å være tilknyttet kalibrering av permeabilitet, oppløsning av sand som følge av installasjon, mangel på full kontakt mellom fundamentlokk og jord samt luftbobler i porevannet. Avviket understreker utfordringen med å fange opp alle egenskapene i den komplekse fundamentoppførselen i en forenklet modell.

Contents

List of Symbols

$\bar{N}$	drainage path ratio
$\bar{Y}^{av}$	normalised stress ratio
$\mathbf{1}$	second order identity tensor
$\dot{\boldsymbol{\epsilon}}$	trend of strain
$\dot{\boldsymbol{\epsilon}}^{acc}$	rate of strain accumulation
$\dot{\boldsymbol{\epsilon}}^{pl}$	plastic strain rate
$\dot{\boldsymbol{\sigma}}'$	trend of effective stress
$\boldsymbol{\sigma}'^{*}$	deviatoric part of effective stress
$\boldsymbol{E}$	elastic stiffness tensor
$\boldsymbol{m}$	direction of strain accumulation
$\dot{\epsilon}^{acc}$	intensity of strain accumulation
$\dot{\epsilon}_q^{acc}$	deviatoric strain accumulation rate
$\dot{\epsilon}_v^{acc}$	volumetric strain accumulation rate
$\dot{f}_N$	function for cyclic preloading (HCA model)
$\dot{f}_N^A, \dot{f}_N^B$	parts A (structural accumulation) and B (basic rate), respectively, of the function for cyclic preloading (HCA model)
ϵ	strain

ϵ^{ampl} strain amplitude

ϵ^{ampl}_{ref} reference strain amplitude

ϵ^{av} average strain

ϵ_a axial strain

ϵ_h, ϵ'_h horizontal stress and horizontal effective stress

ϵ_v, ϵ'_v vertical stress and vertical effective stress

η stress ratio

γ_s shear strain

γ_{sat} saturated unit weight

γ_{unsat} unsaturated unit weight

ν Poisson's ratio

ν_s shear wave velocity

ϕ' friction angle

ϕ'_p peak friction angle

ϕ'_{cv} ultimate value friction angle

ψ dilatancy angle

ρ soil density

σ, σ' total and effective stress

σ_1, σ'_1 major in-plane principal total and effective stress

σ_3, σ'_3 minor in-plane total and effective stress

σ_a axial stress

σ_h,σ'_h horizontal total stress and horizontal effective stress

σ_r radial stress

σ_v,σ'_v vertical total stress and vertical effective stress

τ shear strength

c cohesion

C_u uniformity coefficient

C_v coefficient of consolidation

C_{ampl} HCA model parameter, function f_{ampl}

C_e HCA model parameter, function f_e

C_{N1},C_{N2},C_{N3} membrane penetration correction factors

C_p HCA model parameter, function f_p

C_Y HCA model parameter, function f_Y

d_{10} grain diameter of 10 % passing

d_{60} grain diameter of 60 % passing

D_r relative density

E stiffness

e void ratio

E_{50} average stiffness

E_{50}^{ref} reference average stiffness

e_{max}, e_{min} maximum and minimum pore ratio, respectively

E_{oed} oedometer modulus

E_{oed}^{ref} reference oedometer modulus

e_{ref} reference void ratio

E_{ur} unloading / reloading stiffness

E_{ur}^{ref} reference unloading / reloading stiffness

f_π function for polarization changes (HCA model)

f_{ampl} amplitude function (HCA model)

f_e void ratio function (HCA model)

f_p pressure function (HCA model)

f_Y stress ratio function (HCA model)

G shear stiffness modulus

g^A historiotropic variable (HCA-model)

g_0 initial shear stiffness modulus

h drainage path

k permeability

K_0 initial earth pressure at rest

M inclination of critical state line

p effective mean pressure

p^{av} average effective mean pressure

p_{ref} reference effective mean pressure

q deviatoric stress

q^{av} average deviatoric stress

R_{inter} strength reduction factor

T_v time factor

ϵ^{ampl} strain amplitude

$\rightarrow$ Euclidean norm

m power for stress-level dependency of stiffness

N number of cycles

t time

u pore pressure

Chapter 1

Introduction

1.1 Background

The concept of suction caissons was first reported used in 1958 (Mackereth, 1958). Since then the design of the caisson has improved significantly, however the practical use is mostly limited to installations in the oil and gas industry (Bienen et al., 2018b). As a means to reduce greenhouse emissions and air pollution, today many countries aim to gradually replace energy from fossil fuels with renewable energy sources, such as offshore wind power. In order to do so, the renewable energy sources must be as efficient as possible. As offshore wind farms consist of hundreds of offshore wind turbines and foundations, in contrary to one or just a few structures for more traditional offshore installations, huge economic benefits may be derived from improved foundation concepts (Bienen et al., 2018b).

Cyclic loading effects can be important for all types of offshore structures (Andersen, 2009). Centrifuge experiments at the University of Western Australia (UWA) has studied the cyclic effects of suction caissons. The work is documented in a set of two companion papers in Geotechnique by Bienen et al. (2018a,b): "Suction caissons in dense sand, part I: installation, limiting capacity and drainage" and "Suction caissons in dense sand, part II: vertical cyclic loading into tension". The main findings conclude that cycling into tension is acceptable if compressive average loads are sufficiently large. However, zero or tensile average stress results in unacceptable upward

displacements. The study also investigates the importance of drainage conditions for the caisson response and highlights the complexity of caisson behaviour. These studies have provided valuable insight into the caisson response. However, further studies should aim to understand the relationship between applied cyclic loading, displacements and stress response in addition to drainage and stiffness of the caisson response.

Water saturated sand will during cyclic loading accumulate displacements or pore pressure, or both. The effect of accumulation is accounted for in a high-cycle accumulation (HCA) model for sand described by Wichtmann (2005) and Niemunis et al. (2005). Displacements of suction caissons supporting offshore wind turbines cannot be tolerated due to strict in-service rotational limits (Peire et al., 2009). Additionally, only a small range of frequency is suitable for design as the eigenfrequencies of a single blade and the rotor should be avoided (Bienen et al., 2018b). As the accumulation influences the displacement, and thus the rotation of the caisson, in addition to the soil stiffness, which is decisive for the eigenfrequency of the system, the effects of accumulation must be properly taken into account in design.

Problem Formulation

The thesis focuses on cyclic behaviour of suction caissons and centrifuge experiments performed at the UWA, which is recalculated using PLAXIS. A deeper understanding of the cyclic response of suction caissons supporting offshore wind turbines is essential for improved design. The problem formulations are stated as followed:

1. How is cyclic loading effecting the response of suction caissons supporting offshore wind turbines?

2. How does the simulations based on the centrifuge experiments from the UWA manage to capture the features of the suction caisson response?

1.2 Objectives

The aim of the thesis is to investigate the cyclic response of suction caissons in water saturated dense sand by recalculating a centrifuge experiment at the UWA.

By using theory on the cyclic response of suction caissons supporting offshore wind turbines and the HCA model, the main objectives of this thesis are:

1. Examination of the results from suction caisson experiments performed in a centrifuge at the UWA.
2. Recalculation of the experiments using the finite element program PLAXIS.

1.3 Limitations

The thesis concentrates on centrifuge experiments performed at the UWA. The raw data used to evaluate the experiments contain several different cyclic loading histories. In this thesis, only one of the loading history events is examined. The difference in pore fluid viscosity for this loading cycle is still included in this study. However, no information about initial total stresses or pore pressures are given in the raw data files, which complicates and limits the possibility to recreate the response of the caisson in the simulations.

Due to the complexity of the caisson behaviour and limitations in time, the examination of the HCA model is narrowed down to a literature survey. This means that no simulations or calculations are performed with respect to the HCA model. The recalculation of the centrifuge experiments are therefore exclusively performed with a standard material model, which response may differ from typical cyclic behaviour.

1.4 Scientific Approach

A literature survey has been carried out to develop an understanding of the behaviour of suction caissons for offshore wind turbines. This includes investigation of cyclic behaviour of sand and the HCA model.

Results from centrifuge experiments of a suction caisson in dense sand performed at the UWA have been examined to further understand the behaviour of suction caissons. The examination of the experiments also provides important data for simulations in PLAXIS.

The centrifuge experiments are recalculated in PLAXIS in order to interpret the cyclic response of the suction caisson.

1.5 Outline of the Thesis

The remaining chapters of the thesis are structured as follows:

Chapter 2 gives an introduction to suction caissons and its behaviour in connection to offshore wind turbines.

Chapter 3 describes cyclic behaviour of sand and introduces the high-cycle accumulation model.

Chapter 4 explains how the centrifuge experiments are performed.

Chapter 5 explains the method used for recalculating the centrifuge experiments in PLAXIS.

Chapter 6 presents the results from the centrifuge experiments and PLAXIS simulations.

Chapter 7 gives a discussion on the results from the centrifuge experiments and PLAXIS simulations.

Chapter 8 presents a final conclusion, summary and recommendations for further work.

Chapter 2

Behaviour of Suction Caissons for Offshore Wind Turbines

A suction caisson is best illustrated as an upturned bucket which is lowered into the seabed. The installation process is vital for its functionality, but once the bucket is properly installed, it forms a solid foundation for offshore structures. The interest for the foundation concept seems still to be rising, also for offshore wind turbines. However, compared to more traditional offshore structures, other design criteria and limiting conditions apply for offshore wind turbines.

2.1 Installation and Applications of Suction Caissons

2.1.1 Installation

Suction caissons are more frequently being considered for offshore foundations due to their ease of installation. Shorter installation time, shallower final penetration depth and installation without pile driving make this foundation concept preferred on several occasions rather than more traditional foundation alternatives such as offshore pile foundations (Jia, 2018).

The installation process can be divided into two phases; self-weight penetration and suction installation. The foundation is lowered to the seafloor, and initial penetration of the skirts into

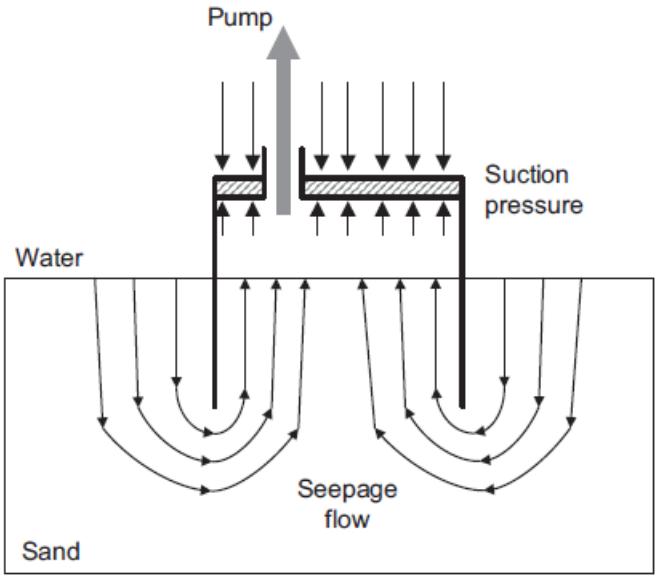

Figure 2.1: Seepage flow with upward gradient on the inside and downward gradient on the outside the caisson caused by suction pressure during installation (Bienen et al., 2018b).

the soil occurs by structural weight. Open valves in the lid allow water inside the caisson to escape. This phase is important as suction assisted penetration cannot be properly performed before a seal between skirt and soil is achieved (Houlsby and Byrne, 2004).

By pumping water from within of the caisson, a negative pressure which drives the foundation into the seabed is created. In sand, the applied suction creates a seepage flow with an upward hydraulic gradient on the inside and a downward gradient on the outside of the caisson. This is illustrated in figure 2.1 The gradient reduces the vertical effective stress at the skirt tip which leaves the tip resistance to almost zero. This contributes significantly to the installation, especially in dense sand (Andersen et al., 2008; Houlsby and Byrne, 2004).

2.1.2 Applications

Suction caissons were first reported used in 1958 in order to support an apparatus for underwater site investigations (Mackereth, 1958). More extensive use of suction caissons in offshore industry began in the 1980s, after offshore oil production had started in the North Sea. The suction caisson was a further development of the design principles used for large gravity-based structures in the North Sea in the middle of the 1970s (Jia, 2018). The Gullfaks C platform was in

1989 installed with 16-meter-large diameter suction caissons penetrating totally 22 meters into the seabed (Tjelta et al., 1990). However, in 1999 the record-breaking Diana platform was installed at 1500 meters depth with a 30-meter-tall suction caisson of diameter 6.5 meters (Bybee et al., 2001), and in 1994 Draupner E proved that suction caissons were not only applicable in soft soils as the platform was installed in dense to very dense sand layers (Bye et al., 1995).

In recent years the usage of suction caissons as foundation for offshore wind turbines has been studied, but the practical experience at full scale is still limited. However, at a test field in Frederikshavn, Denmark, a prototype of a suction caisson supporting an offshore wind turbine was installed on dense sand in 2002 (Ibsen, 2008). In addition monitored suction caissons have been used for met masts at Horns Rev 2 and Dogger Bank (Tjelta, 2015), and at Borkum Riffgrund, Germany, an offshore wind turbine is supported by suction caissons and connected to 126 different sensors from the top of the structure to the suction caisson below seabed (Tjelta, 2015).

It is worth mentioning that structures in the gas and oil industry are typically a one-off installation where improvements in the installation process will have a limited beneficial effect. Wind farms, however, can contain hundreds of wind turbines and may gain huge financial benefits from better foundation design or alternative foundation concepts (Bienen et al., 2018b).

2.2 Limiting Conditions for Offshore Wind Turbines

Compared to the design of traditional structures in the gas and oil industry, offshore wind turbines differ in many important ways. The allowed off-vertical tilt of the offshore wind turbine is limited to 0.25° (Peire et al., 2009), which makes serviceability, rather than capacity, the critical design factor. As deformation of the foundation is the main contributor to rotation of the offshore wind turbine, the effect of cyclic loading on accumulated settlement of the caissons must be carefully considered (Bienen et al., 2018b).

The design of offshore wind turbines needs to avoid the eigenfrequency of both a single blade and the rotor, which results in only a small range of target eigenfrequency. As the foundation stiffness strongly impacts the eigenfrequency of the system, it is important to carefully study its

behaviour (Bienen et al., 2018b). The stiffness might be affected due to large number of applied load cycles, and accumulation of stiffness should therefore be an important part of that study. Changes in the soil stiffness over 25 years of design life for offshore wind turbines makes it very complicated to choose a single stiffness to represent the foundation response in structural analyses (Bienen et al., 2018a).

Offshore wind turbines are also much lighter and will experience bigger horizontal and moment loads compared to traditional offshore structures. The turbine superstructures can be supported by one single caisson or a group of three or four caissons. For multi-caisson foundation systems, each caisson will experience different loads depending on the metocean conditions and the direction of loading, see figure 2.2 and 2.3. When subjected to wind loads, the leeward caisson is heavily loaded, while the windward caisson is lightly loaded. The lightly loaded caisson can be exposed to cyclic loading into tension, and might therefore be the limiting design condition (Bienen et al., 2018b).

It is evident that upward permanent displacement must be avoided. When the caisson is pushed down, the soil will become stronger and stiffer, and resistance against downward deformations will become larger. This is not the case for upward displacement. When pulled upward the penetration depth is reduced, the caisson's lid might lose contact with the soil plug, the resistance against further displacement becomes smaller and the structure may collapse. To protect structures against this type of displacement, the tensile loading has in general been limited to the frictional capacity (Houlsby, 2016).

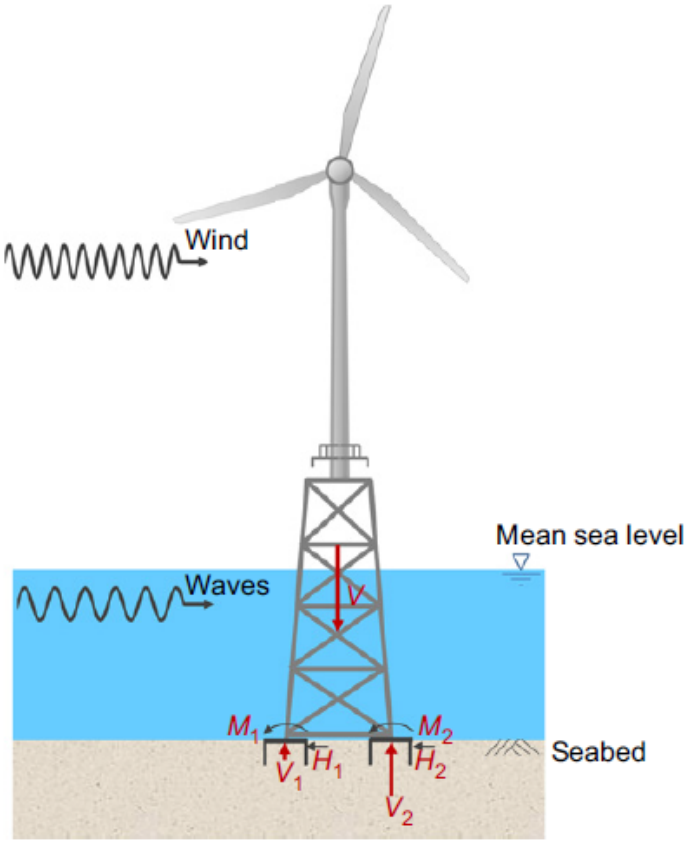

Figure 2.2: The figure illustrates how the load direction is decisive for what kind of loads the different caissons will experience (Bienen et al., 2018a).

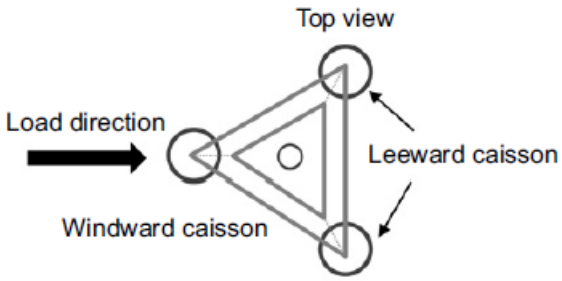

Figure 2.3: A top view of three caissons supporting an offshore wind turbine (Bienen et al., 2018b).

Chapter 3

Cyclic Behaviour of Sand and the HCA Model

Offshore installations are typically exposed to cyclic loads due to wind and waves. In order to fully understand the cyclic behaviour of suction caissons, it is important to study soil mechanics relevant for this foundation concept. This chapter describes both the important soil features of monotonic and cyclic loading. In addition, the main concept of the high-cycle accumulation (HCA) model is examined.

3.1 Cyclic Behaviour of Sand

Cyclic loading may cause accumulation of pore pressure and deformation. This occurs not only due to large strains, but also for large numbers of cycles with small strain-amplitudes. During drained loading, every load cycle causes a small change in the soil structure which increases the soil displacement. For undrained cyclic loading the pore pressure build-up reduces effective stresses, and the soil stiffness and shear strength will therefore decrease. In extreme cases this can cause soil liquefaction and loss of the overall stability (Niemunis et al., 2005).

Important soil mechanics applicable to suction caissons in sands are presented by Bye et al. (1995). The essence from Bye's paper is provided in this section (3.1).

3.1.1 Monotonic Loading

The soil shear strength of saturated soil, τ, is given by the effective stress, σ', and frictional angle, ϕ':

$$\tau = \sigma' tan\phi' \tag{3.1}$$

When a load is applied to the soil, it is carried by solid grains and pore water pressure. The rate of applied loading determines the size of excess pore water pressure. Considering an idealised elastic, non-dilatant soil, it will not experience any change in mean effective stress due to an instantaneous change of load. However, the pore water pressure will change instantaneous, and a non-isotropic stress increment will result in a change in shear stresses. Despite this, the soil strength will not be affected.

Dissipation of the induced pore water pressure over time generates changes in effective stresses and thus changes in the soil strength. With the passage of time, a compression load on bucket foundation will cause the mean effective stress to increase, and hence the soil strength. Likewise, a tension load will lead to decrease in mean effective load and reduction of soil strength with time. This is the reason why caution is necessary when designing offshore wind turbines with respect to tensile loads, see section 2.2. Finally, when all induced pore pressure is fully dissipated, the small contribution from friction on the skirt walls is the only resistance against tensile loads.

The idealisation of elastic and non-dilatant soil are generally not applicable for real soils. Observations show that the soil either contract or dilate. Very dense sand, which is further examined, will in general dilate and loose sand contracts. The phenomenon where neither contractancy nor dilatancy occur, i.e. no volume change during shearing, is called "critical state" and takes place for one particular mean stress and void ratio.

When water flow is insufficient, the expansion due to dilatant behaviour of soil is prevented by the incompressible nature of water due to suction. In addition, the mean effective stress increases and thus the shear strength. The true limiting strength is not reached until soil effective stresses and density have changed so much that the critical state is achieved. The term “steady

state" strength is used to describe the equivalent phenomenon limited to fully undrained behaviour. For this type of behaviour, the cavitation pressure must also limit the strength. This is the level of vacuum pressure where water vaporises, and can occur due to a rapid change of pressure.

3.1.2 Cyclic Loading

Bucket foundations are mainly subjected to cyclic loads. This type of loading results in another very important mechanism; pore pressure accumulation. The soil matrix of all sands, even the densest, will tend to contract during cyclic undrained loading and hence accumulate pore pressure. This type of sand with very high bulk stiffness can generate huge pore pressures. However, for dense sand to reach the same level of pore pressure accumulation as initially looser sand, the amplitude of the load cycles must be larger and more numerous compared to lose sands.

In the extreme case "initial liquefaction" occurs when the pore pressure build-up reduces the soil mean effective stress to zero, which consequently leads to a huge reduction in shear stiffness. Very dense sands will, when sheared to large enough strains, recover the lost stiffness. However, the permanent strains may be way larger than tolerated.

Cyclic loading may cause irreversible strains under conditions less extreme than initial liquefaction. Soil particles tend to rearrange during repeated cyclic loading, even when the amplitude is low. The connections between the soil grains may collapse and the contact area and tension between the grains change. Even though these changes might be infinitesimal, the effect is noticeable on the deformation after hundreds or thousands load cycles (Zhou and Chen, 2005). This type of displacement as a result a large number of cycles is accumulated deformation.

3.2 High-Cycle Accumulation Model

The purpose of high-cycle accumulation (HCA) models is to calculate settlements or stress relaxation in soils due to a combination of average loads and large numbers of small-strain cyclic loads. The HCA model also takes the accumulation of pore pressure during cyclic loading of water saturated sand under nearly undrained conditions into account (Wichtmann et al., 2010).

The HCA model described in detail by Niemunis et al. (2005) and (Wichtmann, 2005) is based on the fundamental idea that an oscillating part and a trend part can describe the stress and strain paths generated by high-cyclic loading. The main focus of the model is the trend part, which is predicted by accumulation of strain, $\dot{\epsilon}^{acc}$, while the oscillating part is represented by the strain amplitude, ϵ^{ampl}. The cumulative trend can either consist of small residual strains (pseudo-creep) or residual stresses (pseudo relaxation), and is related by the following formula:

$$\dot{\boldsymbol{\sigma}}' = \boldsymbol{E} : (\dot{\boldsymbol{\epsilon}} - \dot{\boldsymbol{\epsilon}}^{acc} - \dot{\boldsymbol{\epsilon}}^{pl}) \tag{3.2}$$

where $\dot{\boldsymbol{\sigma}}'$ is the effective stress rate, $\boldsymbol{E}$ is the elastic stiffness tensor, $\dot{\boldsymbol{\epsilon}}$ is the rate of stain, $\dot{\boldsymbol{\epsilon}}^{acc}$ is the accumulated strain rate and $\dot{\boldsymbol{\epsilon}}^{pl}$ is the rate of plastic strain. Compression is here defined as positive, both for stress and strain. Note that when studying high cycles models the term “rate” refers to the derivative with respect to number of cycles, N, and not time, t.

To estimate the accumulation due to high cyclic loads a combination of a special explicit calculation strategy, a HCA model and finite element analysis may be used.

3.2.1 Explicit Calculation Strategy

For low-cycle load problems, pure implicit calculation strategies such as elastoplastic multi-surface models or endochronic models are normally used. However, these methods give numerical errors when applied to large number of cycles (Niemunis et al., 2005). An explicit strategy usable for high-cyclic loads calculate only a small number of cycles implicitly. The main part of the cycles are calculated explicitly by calculating the accumulation of strain directly. A packet of

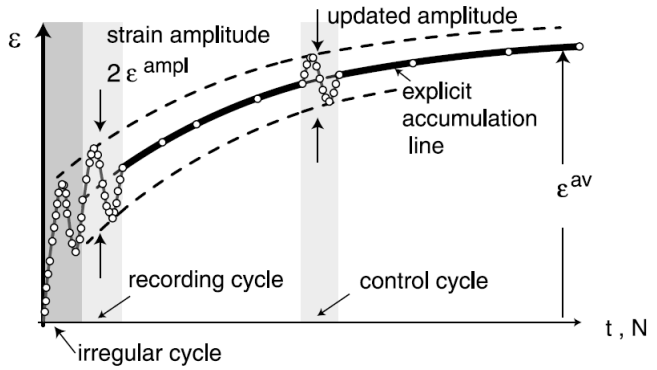

Figure 3.1: The basic idea of a combined implicit and explicit calculation. The horizontal axis is time, t, for implicit calculations and number of cycles, N, for explicit calculations (Niemunis et al., 2005).

ΔN cycles with a given amplitude, ϵ^{ampl}, generates an irreversible strain, $\dot{\boldsymbol{\epsilon}}^{\boldsymbol{acc}}\Delta N$, where $\dot{\boldsymbol{\epsilon}}^{\boldsymbol{acc}}$ is given in equation 3.3. A special constitutive formulation, such as the HCA model, is required to be able to treat packets of cycles. This type of calculation is similar to creep calculations in viscoplastic models, substituting Δt for ΔN (Wichtmann et al., 2010)

During the explicit calculations the strain amplitude, ϵ^{ampl}, is constant. However, after thousands of cycles the strain amplitude may need to be "updated" due to compression of the soil and redistribution of forces. As shown in figure 3.1, an implicit calculation should be performed between the explicit calculations in order to correct or update the strain amplitude. This is of importance as the strain amplitude is an essential input parameter to the HCA model (Wichtmann et al., 2010).

3.2.2 Parameters in the HCA Model

The rate of accumulation, $\dot{\boldsymbol{\epsilon}}^{\boldsymbol{acc}}$, in equation 3.2 is given by

$$\dot{\boldsymbol{\epsilon}}^{\boldsymbol{acc}} = \dot{\epsilon}^{acc}\boldsymbol{m} \tag{3.3}$$

where $\boldsymbol{m}$ describes the direction of accumulation and $\dot{\epsilon}^{acc}$ is the intensity of strain accumulation. Drained cyclic triaxial tests show good correlation with approximation from the flow rule of the modified Cam-clay model and thus the ratio between volumetric strain, $\dot{\epsilon}_v^{acc}$, and deviatoric

strain, $\dot{\epsilon}_q^{acc}$. As this approximation is used in the HCA-model, $\boldsymbol{m}$ is given as

$$\boldsymbol{m} = \left[\frac{1}{3}(p - \frac{q^2}{M^2 p}\mathbf{1} + \frac{3}{M^2}\boldsymbol{\sigma}'^*\right]^{\rightarrow} \tag{3.4}$$

where the subscript arrow indicate Euclidean norm, $\mathbf{1}$ is the second order identity tensor and $\boldsymbol{\sigma}'^*$ denotes the deviatoric part of the effective stresses. The effective mean pressure, p, and deviatoric stress, q, are for drained triaxial tests given as $p = (\sigma'_1 + 2\sigma'_3)/3$ and $q = \sigma'_1 - \sigma'_3$. The inclination of the critical state line is $M = \frac{6sin\phi}{3 \pm sin\phi}$.

The intensity of strain accumulation, $\dot{\epsilon}^{acc}$, is given by six independent functions, see equation 3.5, which account for different influencing parameters.

$$\dot{\epsilon}^{acc} = f_{ampl}\dot{f}_N f_e f_p f_Y f_\pi \tag{3.5}$$

The effect of strain amplitude, ϵ^{ampl}, is expressed by f_{ampl}, while f_π expresses the effect of polarisation. For constant polarisation $f_\pi = 1$. Increase of average stress ratio, $\eta = \frac{q^{av}}{p^{av}}$, and reduction of mean pressure, p^{av} , will cause $\dot{\epsilon}^{acc}$ to increase, and this is predicted by the functions f_p and f_Y. Increasing void ratio, e, described by f_e, results in increasing $\dot{\epsilon}^{acc}$. Cyclic preloading and its dependency on $\dot{\epsilon}^{acc}$ are captured by the function $\dot{f}_N = \dot{f}_N^A + \dot{f}_N^B$. The preload is dependent on number of cycles and their amplitude, and the model quantify this by

$$g^A = \int f_{ampl}\dot{f}_N^A dN \tag{3.6}$$

which is included in $\dot{f}_N$. The accumulation curves, $\epsilon^{acc}(N)$, is proportional to $f_N = C_{N1}[ln(1 + C_{N2}N) + C_{N3}N]$ for cycles of constant amplitude.

A summary of functions and constants in addition to example values of constants for $N = 10^5$ cycles are given in table 3.1.

The parameters of the HCA model are described in more detail by Niemunis et al. (2005) and Wichtmann (2005). Due to time limitations in the project period of the master thesis, the study of the HCA-model is limited to this literature survey.

Table 3.1: Functions and constants used in the HCA model to determine $\dot{\epsilon}^{acc}$ for $N = 10^5$ cycles for a medium-coarse sand (adapted from Wichtmann, 2005).

Parameter	$N = 10^5$
$f_{ampl} = min\left\{\left(\frac{\epsilon^{ampl}}{\epsilon^{ampl}_{ref}}\right)^{C_{ampl}}; 100\right\}$	
ϵ^{ampl}_{ref}	10^{-4}
C_{ampl}	2.0
$\dot{f}_N = \dot{f}^A_N + \dot{f}^B_N$, where	
$\dot{f}^A_N = C_{N1}C_{N2}exp\left[-\frac{g^A}{C_{N1}f_{ampl}}\right]$	
$\dot{f}^B_N = C_{N1}C_{N3}$	
C_{N1}	3.6×10^{-4}
C_{N2}	0.43
C_{N3}	5.0×10^{-5}
$f_p = exp\left[-C_p\left(\frac{p^{av}}{p^{ref}} - 1\right)\right]$	
C_p	0.43
p_{ref} [kPA]	100
$f_Y = exp(C_Y \bar{Y}^{av})$	
C_Y	2.0
$f_e = \frac{(C_e-e)^2}{1+e}\frac{1+e_{ref}}{(C_e-e_{ref})^2}$	
C_e	0.54
e_{ref}	0.874
For constant polarisation	
$f_\pi = 1$	

Chapter 4

Centrifuge Experiments of Suction Caissons in Sand

To develop better insight into the cyclic behaviour of suction caissons in dense sand, a series of centrifuge experiments are performed at the University of Western Australia (UWA), and described in detail in a set of two companion papers in Geotechnique by Bienen et al. (2018a,b): "Suction caissons in dense sand, part I: installation, limiting capacity and drainage" and "Suction caissons in dense sand, part II: vertical cyclic loading into tension". A model caisson simulates one of the three suction caissons supporting an offshore wind turbine on a jacket support structure. The main focus of the research is on performance during installation, response to cyclic loading and caisson extraction behaviour.

To achieve soil stresses similar those of the prototype, all tests are conducted in a beam centrifuge at an acceleration of 100 g. The samples are composed of extremely dense Baskarp sand and saturated with high viscosity pore fluid of 100 cSt or 660 cSt.

4.1 Measurements and Equipment

The model caisson made of aluminium with 40 mm skirt length, 0.5 mm skirt thickness and a diameter of 80 mm is equivalent to a prototype caisson with 4 m skirt length, 50 mm skirt thick-

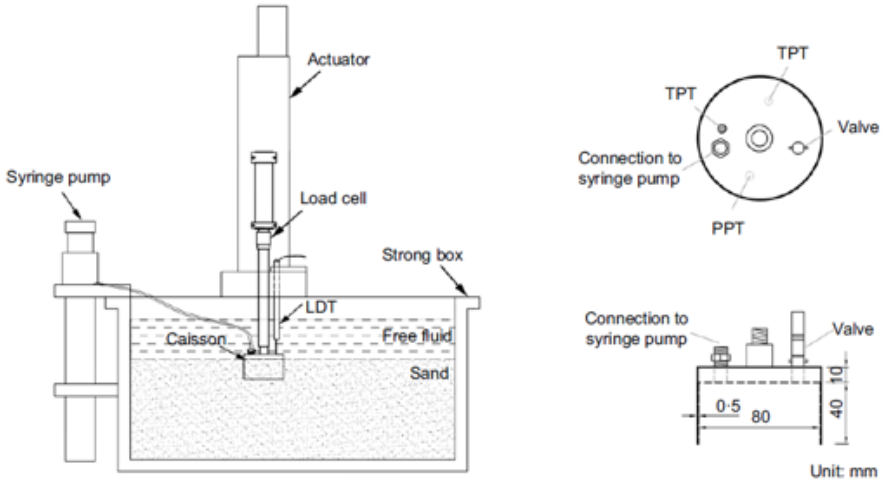

Figure 4.1: Illustration of the model caisson, equipment and arrangement used during testing at UWA (Bienen et al., 2018b).

ness and a diameter of 8 m. During testing the soil samples were covered by a 70 mm layer of fluid. The caisson lid invert is equipped with a pair of total and pore pressure transducers, and the fluid pressure at the top of the caisson lid is measured with an additional total pressure transducer. The displacement of the caisson is continuously recorded by a Linear Displacement Transducer (LDT). Figure 4.1 show an illustration of the model caisson, its equipment and arrangement (Bienen et al., 2018b).

4.2 Cyclic Loading

Cyclic loads are applied under conditions representing an offshore wind turbine at 40 m water depth in the North Sea as shown in figure 4.2. As the soil samples are covered by a layer of 70 mm, the water depth of 40 m is assumed to only represent load conditions, and not the actual water depth in the experiments. The model experiments aim to represent in situ conditions as closely as possible by completing self-weight installation, suction assisted penetration, cyclic loading and caisson extraction. The testing procedure is schematically shown in figure 4.3. The cyclic frequency of 0.5 Hz was kept constant, and by altering the mean load and cyclic amplitude a collection of different results was produced. Several of the experiments were cycled into tension, and the effect of this is of special attention.

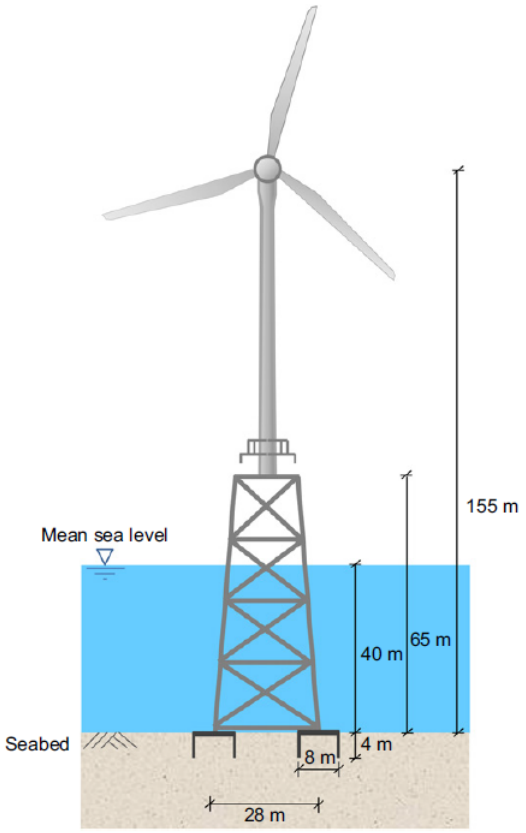

Figure 4.2: The applied cyclic loading aim to represent loads from an offshore wind turbine at 40 m water depth in the North Sea (Bienen et al., 2018b).

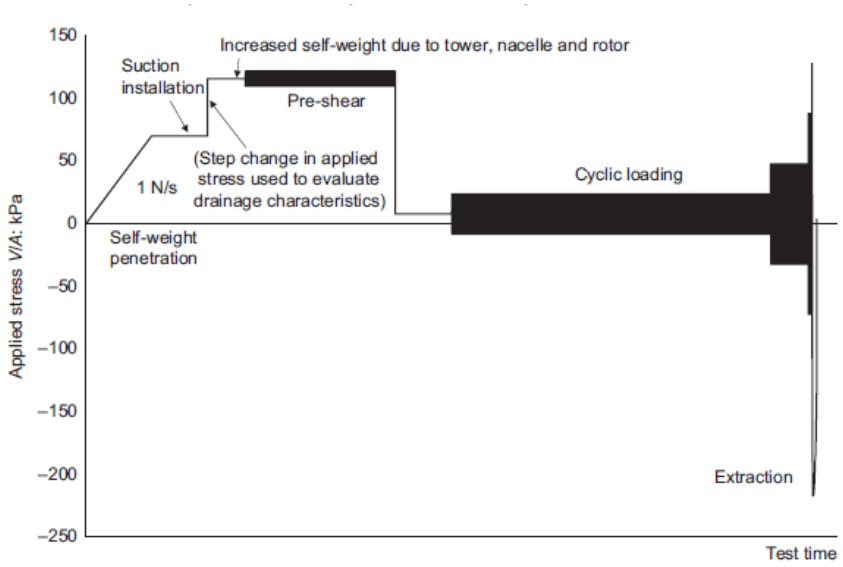

Figure 4.3: The testing procedure of the experiments at UWA schematically presented (Bienen et al., 2018b).

4.3 Material Parameters

The minimum and maximum void ratios are measured to be $e_{min} = 0.57$ and $e_{max} = 0.86$, using the procedure described by Blaker et al. (2015). The grain size distribution is shown in figure 4.4, and the uniformity coefficient, $C_u = \frac{d_{60}}{d_{10}}$, is 1.61. Andersen and Jostad (1999) uses initial earth pressure at rest, $K_0 = 0.54$, and unsaturated dry unit weight, $\gamma_{unsat} = 11 KN/m^3$ in their analysis of Baskarp Sand.

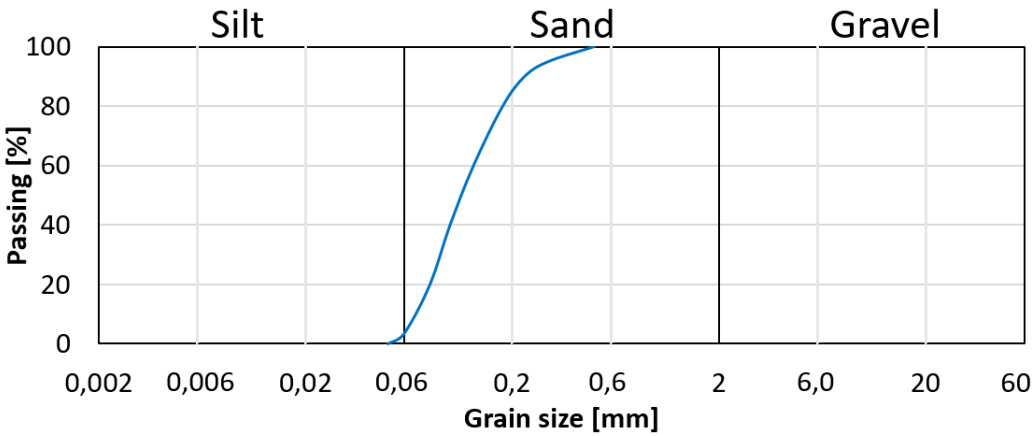

Figure 4.4: The grain-size distribution of Baskarp sand is similar to typical North Sea sands (adapted from Andersen (1989)).

The peak friction angle, ϕ'_p, for drained triaxial tests is measured to be 44.5° and reduces to 34.5° for ultimate value fraction angle, ϕ'_{cv} (Andersen and Berre, 1999). "cv" denotes constant volume, and ϕ'_{cv} represents the friction angle for large strains in which the volume remains constant despite additional strains. Figure 4.5 shows an example of how the friction angle changes with strains for loose and dense sands and illustrate the definition of ϕ'_p and ϕ'_{cv}.

In addition, Andersen and Berre (1999) measured a permeability of $k = 8.04 \times 10^{-5}$ m/s for a water-saturated sample with relative density of $D_r = 95\%$. This density is close to the centrifuge samples, which have a relative density of $D_r = 98 \pm 2\%$.

The samples saturated with 660 cSt pore fluid aim to show a close to undrained behaviour, while the samples with 100 cSt silicon oil are expected to be partially drained. The difference in consolidation characteristics for the two pore fluids is presented in figure 4.6, illustrating pore pressure dissipation time histories after a load change.

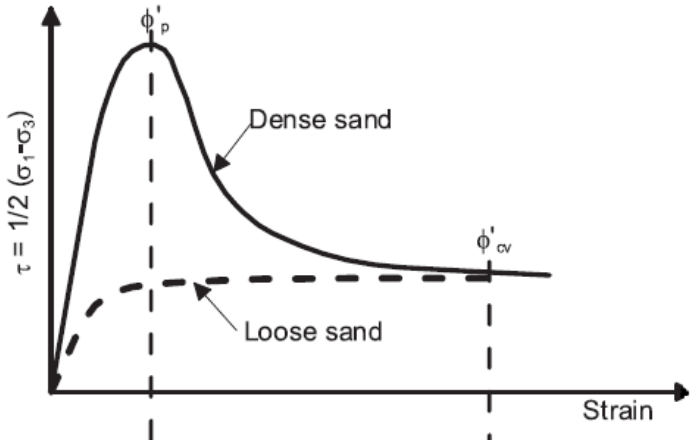

Figure 4.5: Definition of peak friction angle, ϕ'_p, and ultimate friction angle, ϕ'_{cv}, in drained tests on loose and dense sands (Andersen and Schjetne, 2012).

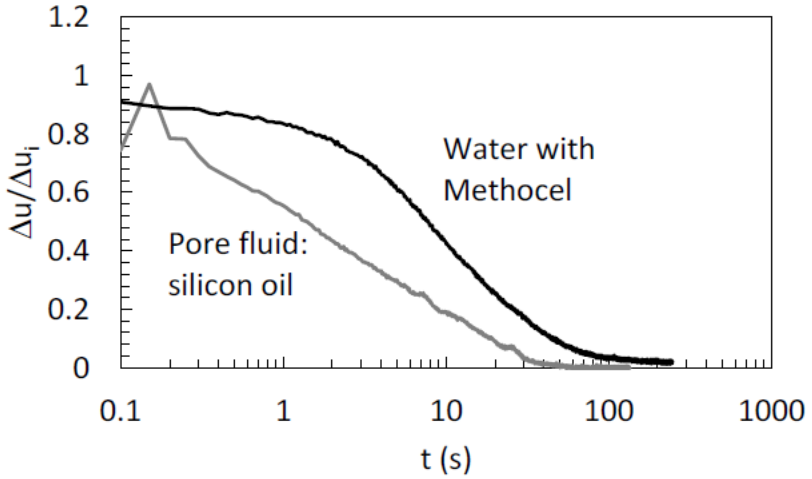

Figure 4.6: Difference in consolidation characteristics for the two pore fluids. The horizontal axis represents time in seconds on a logarithmic scale, while the vertical axis illustrates normalised pore pressure (Bienen et al., 2018b).

4.4 Extraction Resistance

To measure the pull-out capacity of the caisson, extraction has been conducted at a rate of 0.001 mm/s and 3 mm/s to determine drained and undrained behaviour, respectively. At full skirt penetration the drained tensile capacity for test with lower viscosity fluid was measured to be approximately 15 kPa, while the more undrained behaviour has a tensile resistance of approximately 150 kPa. The results for higher viscosity fluid are approximately 30 kPa for drained behaviour and 200 kPa for undrained behaviour. This difference in pull-out capacity for different viscosity fluids indicates that the behaviour is neither fully drained nor fully undrained, which means that drainage parameters effect the results of tensile capacity.

Chapter 5

Recalculation of Centrifuge Experiments in PLAXIS

The model experiments performed at UWA are in this study recalculated using the finite element software, PLAXIS 2D. This chapter explains how the simulations are performed in PLAXIS and presents the input parameters.

5.1 Structure of the Model

An axisymmetric model in PLAXIS 2D is used to model the suction caisson from experiments at UWA, described in chapter 4, in prototype scale. The caisson consists of a 1 m thick lid to assure that the caisson lid is stiff enough, and a 5 cm thick skirt. The lid is modelled 4 m long, which results in a lid diameter of 8 m because of symmetry. The skirt wall is 4 m tall. The caisson is made of linear elastic weightless non-porous material with properties suitable for aluminium, which is given in table 5.1. The soil cluster around the caisson represents the strong box in figure 4.1. Figure 5.1 shows a screenshot of the PLAXIS model. The skirt wall is covered in interfaces with properties calibrated from drained extraction resistance tests.

Table 5.1: Material parameters for caisson made of aluminium.

$E\ [kN/m^2]$	70×10^6
$\nu\ [-]$	0.34
$G\ [kN/m^2]$	26.12×10^6
$E_{oed}\ [kN/m^2]$	107.7×10^6

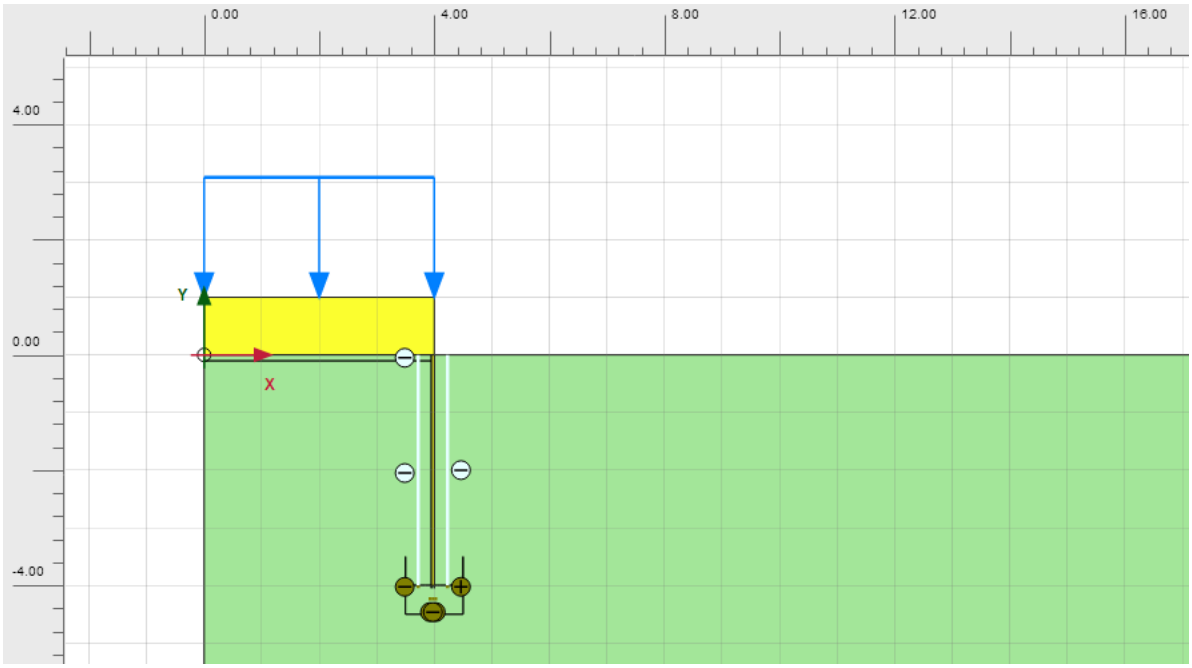

Figure 5.1: A screenshot shows the caisson of the PLAXIS model used in the PLAXIS simulations.

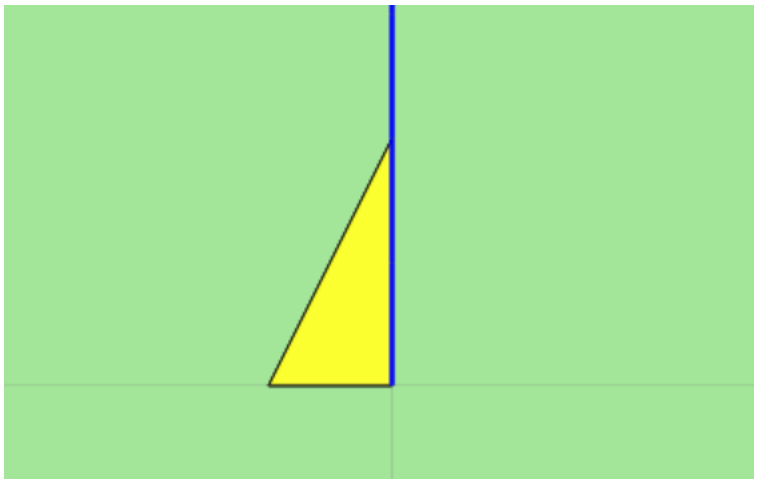

Figure 5.2: A screenshot shows a triangle added to the bottom of the caisson skirt to account for the thickness of the skirt. The triangle is 5 cm at the bottom.

A simpler model where the caisson lid and skirt are made of stiff beam elements is also considered. This model is for instance used to calibrate drained extraction resistance. To include thickness at the skirt tip, a soil triangle with stiffness similar to the aluminium skirt can be added at the bottom of the skirt beam as shown in figure 5.2. An advantage using this model is reduction in required capacity needed to perform the calculation. This is due to the simpler construction of caisson skirt and lid which require a less complicated mesh generation for the finite element analysis. However, the capacity of most of today's computers is large enough to handle the extra iterations needed. In addition, the triangle can cause false moment because of its non-symmetry. The model first introduced is therefore mainly used in the simulations.

5.1.1 Finite Element Mesh

The model is not very sensitive to elements size. Figure 5.3 illustrates the displacement response for an arbitrary soil exposed to cyclic loading similar to the centrifuge experiments. Simulations are performed using "very fine" and "very coarse" element distribution, and the difference in the response is limited. "Coarse" element distribution is therefore considered as fine enough for the further simulations. However, the soil around at the skirt tip is exposed to great stress, and the soil response there is very important. As seen in figure 5.4, additional points are added around the skirt tip to refine the mesh here. An overview of the mesh is shown in figure 5.5.

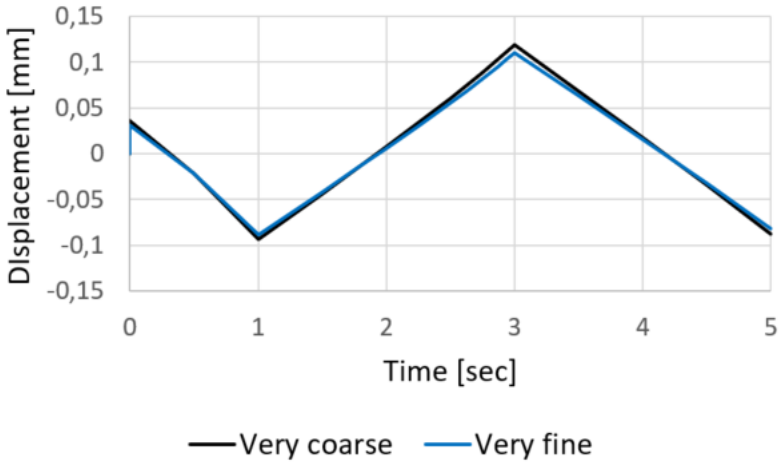

Figure 5.3: The dependency of element size on displacement. "Very fine" and "very coarse" element distributions are shown in the figure.

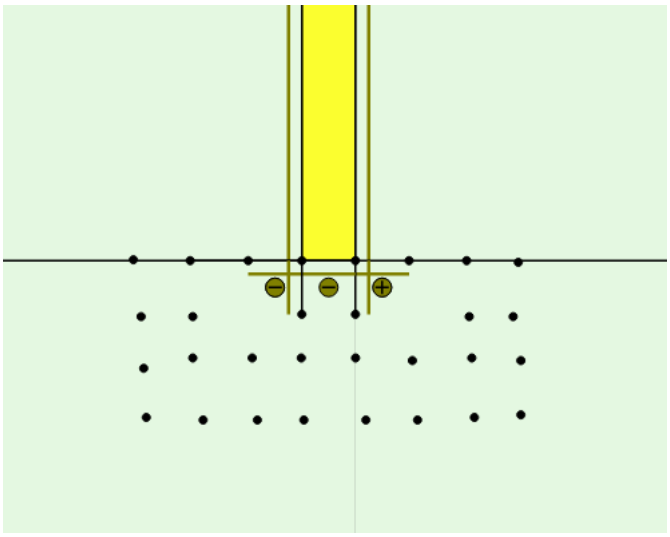

Figure 5.4: The figure shows the points around the skirt tip which contribute to refining of the mesh.

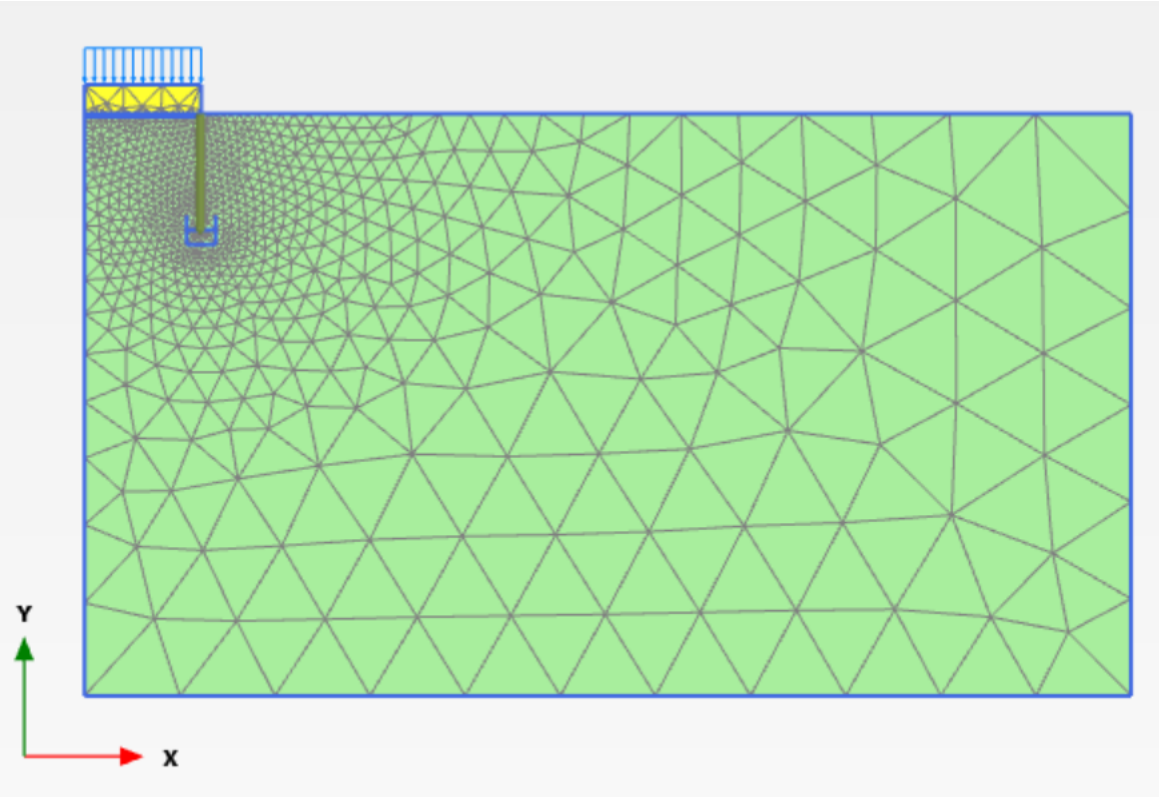

Figure 5.5: An overview of the mesh used in the calculations.

5.1.2 Variations of the Model

To account for a different soil behaviour at the skirt tip compared to the rest of the soil, a soil cluster around the skirt tip can be replaced by another material. The cluster, which is 1 m wide and 0.5 m tall, is shown in figure 5.6.

A thin layer just beneath the caisson lid can also be replaced by another material. This is done to take account of a possible water pocket beneath the caisson lid. The layer in the PLAXIS model is 10 cm thick, as long as the caisson lid and shown in figure 5.7.

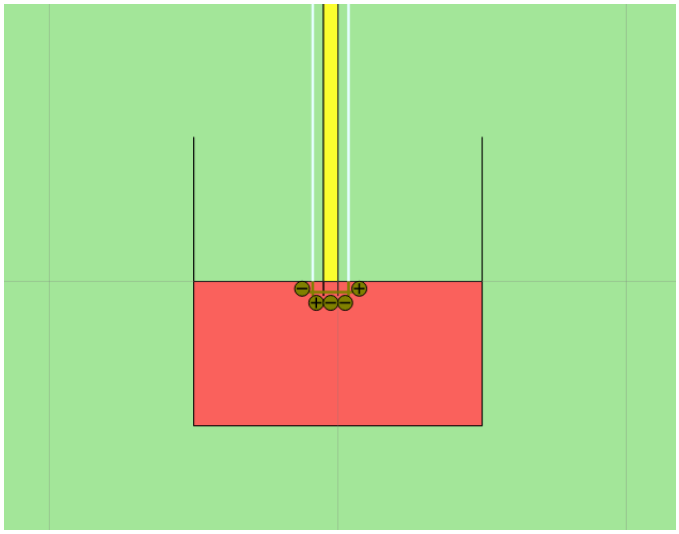

Figure 5.6: A cluster representing another material around the skirt tip.

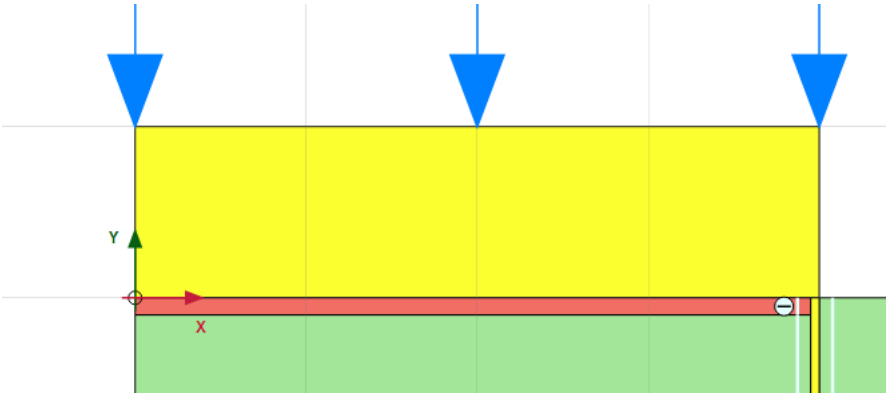

Figure 5.7: A thin layer of another material representing a water pocket just beneath the caisson lid.

5.1.3 Calculation Types and Loading

The simulations in PLAXIS are conducted using different calculation types; plastic or consolidation calculation. The plastic analyses are either fully drained or fully undrained. For all types of calculations, the load is applied in several phases. Initially the mean stress is applied drained. Subsequently a distributed load corresponding to the maximum applied compression stress is applied, which marks the start of the cyclic loading. The soil is thereafter unloaded to its mean stress, and further to its maximum load in tension. As the aim is to study the behaviour during unloading and reloading, the soil must have experienced the current applied load earlier. To satisfy this condition, the soil is once again loaded to its maximum compression load.

The consolidation calculations are supposed to represent the centrifuge experiments most precisely. The cyclic load is therefore applied with a frequency of 0.5 Hz which is similar to the centrifuge experiments. This is accomplished by splitting one cyclic into four quarters and assign one phase two each quarter. The time interval of each phase is set to 0.5 seconds. The same response would have been possible to achieve by splitting the cycle in two. However, the use of four phases per cycle makes it a lot easier to separate the response in tension and compression.

A displacement node and a stress point are selected next to the symmetry line, right below the caisson lid. All results are based on responses in this node or stress point, which exact locations are shown in figure 5.8.

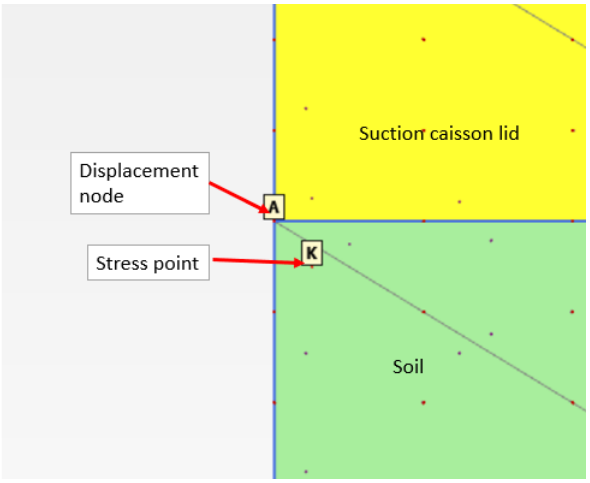

Figure 5.8: Exact position of displacement node and stress point.

5.2 Adaption of Parameters

5.2.1 Stiffness Parameters for the Hardening Soil Model

The stiffness parameters E and m are determined by simulating basic soil lab tests in the *Soil-Test* option in PLAXIS. In a report from Norwegian Geotechnical Institute (NGI) by Andersen and Jostad (1999), a set of oedometer and triaxial tests performed on dense Baskarp sand are presented. The results from these tests are reproduced as identically as possible by adjusting stiffness parameters of the hardening soil model.

An oedometer test conducted on Baskarp sand with relative density $D_r = 85$ %, is here assumed to have $OCR = 1$. A very good match between the results from the laboratory test and PLAXIS simulation is achieved for the parameters listed in table 5.2. The estimation is illustrated in figure 5.9. The result from the oedometer tests from Andersen and Jostad (1999) is here simplify as the curve in reality has a different path for unloading and reloading. This would have been visible at the curve from the oedometer test around $\sigma'_v = 200$ kPa. However, the difference in the unloading and reloading path is not captured by the hardening soil model.

The unloading stress path is dependent on the stress level of the soil prior to the unloading. Consequently, the two unloading curves for the oedometer experiment in figure 5.9 have different slopes. The unloading-reloading stiffness, E_{ur}, is chosen to overestimate the stiffness of the low-stress unloading path and underestimated the initial part of high-stress unloading path.

The two triaxial compression tests are anisotropically consolidated with vertical consolidation stress $\sigma_v = 250$ kPa and horizontal consolidation stress $\sigma_h = 112.5$ kPa. The vertical stress increases while the horizontal stress is kept constant during the tests. The results from the drained and undrained tests are illustrated in figure 5.10 and 5.11, respectively. The stiffness parameters are given in table 5.2. The reference stiffness for unloading and reloading, E_{ur}^{ref}, is chosen arbitrary as the soil specimens are not exposed to this type of loading.

An undrained triaxial extension test has been conducted by Andersen (1989). The anisotropic consolidation is identical to the triaxial compression test, i.e. $\sigma_v = 250kPa$ and $\sigma_h = 112.5kPa$. The test is run by keeping the horizontal stress constant while reducing the vertical stress. The result from the soil test is shown in figure 5.12.

Table 5.2: Combination of E_{50}^{ref}, E_{oed}^{ref}, E_{ur}^{ref} and m which gives the curves in figure 5.9-5.12. The material model used is the hardening soil model.

Oedometer, $D_r = 85,0\%$

E_{50}^{ref}	120 MPa
E_{oed}^{ref}	110 MPa
E_{ur}^{ref}	500 MPa
m	0,25

Drained triaxial compression, $D_r = 96.2$

E_{50}^{ref}	92.5 MPa
E_{oed}^{ref}	70 MPa
E_{ur}^{ref}	500 MPa
m	0.5

Undrained triaxial compression, $D_r = 91.7$

E_{50}^{ref}	250 MPa
E_{oed}^{ref}	237 MPa
E_{ur}^{ref}	500 MPa
m	0.3

Undrained triaxial extension, $D_r = 95.0$

E_{50}^{ref}	175 MPa
E_{oed}^{ref}	203 MPa
E_{ur}^{ref}	500 MPa
m	0.525

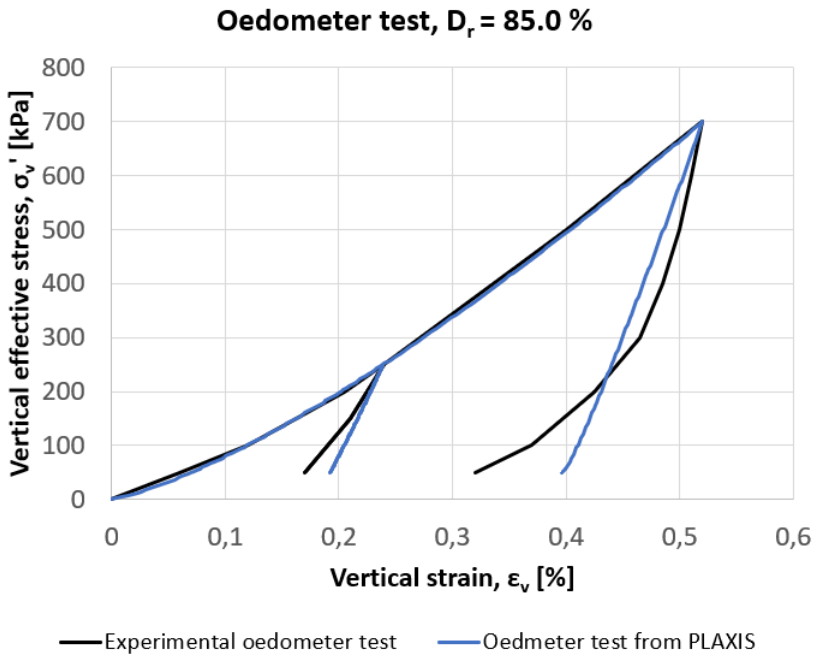

Figure 5.9: A comparison between oedometer test from experiments and *SoilTest* in PLAXIS. Stiffness parameters for the hardening soil material used in PLAXIS are shown in table 5.2.

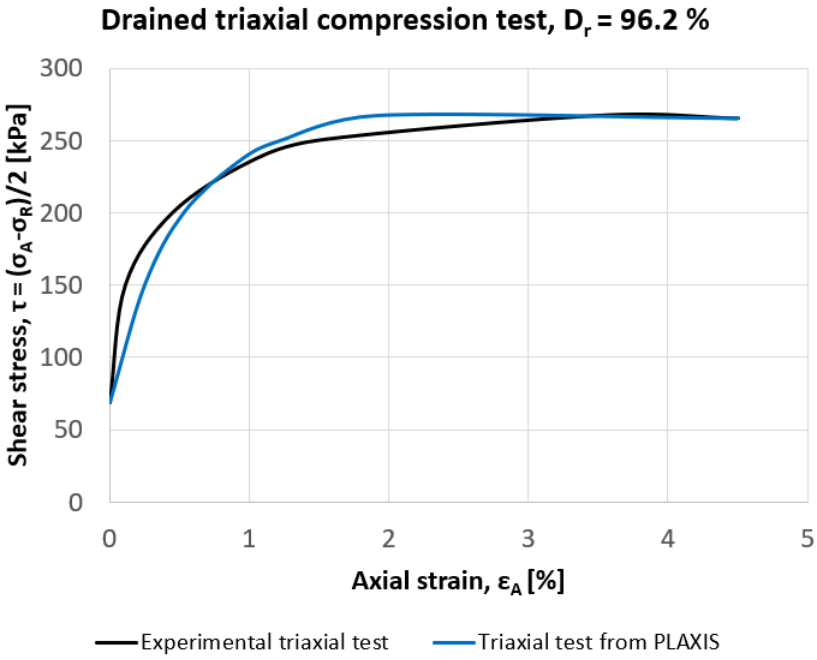

Figure 5.10: A comparison between triaxial drained compression test from experiments and *SoilTest* in PLAXIS. Stiffness parameters for the hardening soil material used in PLAXIS are shown in table 5.2.

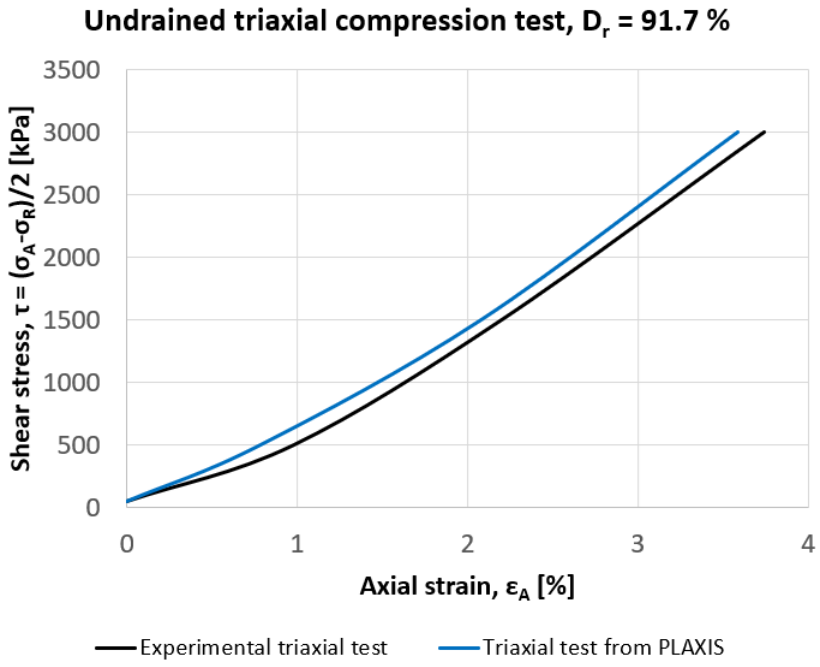

Figure 5.11: A comparison between triaxial undrained compression test from experiments and *SoilTest* in PLAXIS. Stiffness parameters for the hardening soil material used in PLAXIS are shown in table 5.2.

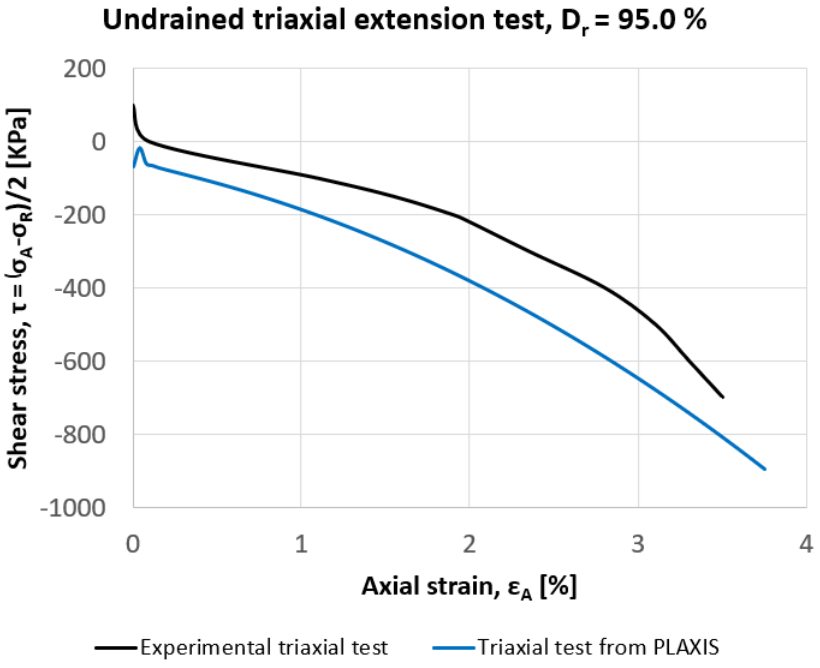

Figure 5.12: A comparison between triaxial undrained extension test from experiments and *SoilTest* in PLAXIS. Stiffness parameters for the hardening soil material used in PLAXIS are shown in table 5.2.

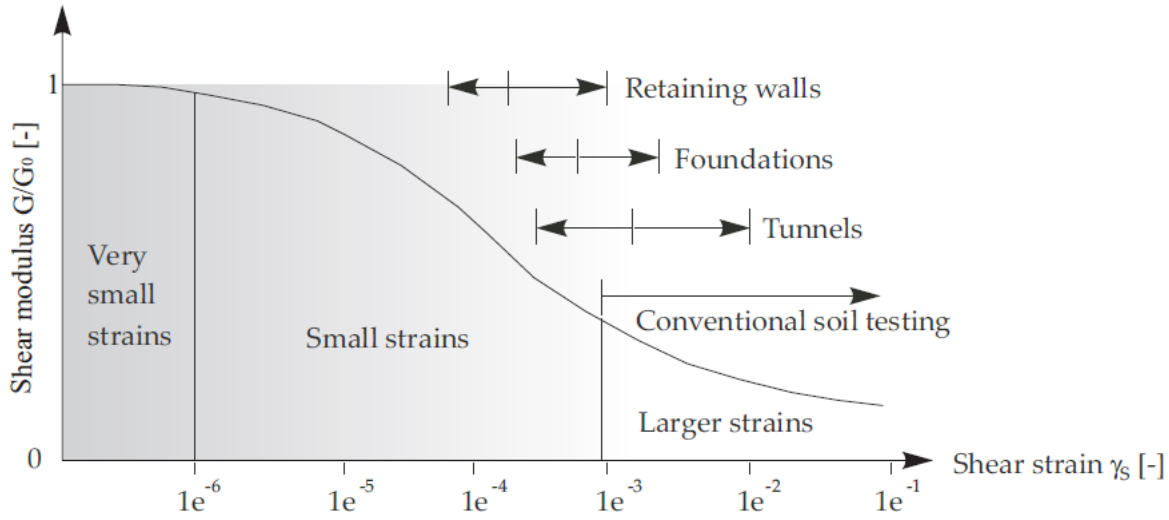

Figure 5.13: Non-linearly dependency of soil stiffness on strain amplitude (Brinkgreve et al., 2017).

5.2.2 The Hardening Soil model with Small-Strain Stiffness

For an arbitrary soil the initial stiffness, which means the stiffness at very small strain rates, is higher than the average stiffness, E_{50}. This is due to the dependency of stiffness on applied strain. Figure 5.13 illustrates that for conventional testing, such as oedometer and triaxial tests, the stiffness of the soil is often reduced to less than half its initial value at the range of strain that is possible to measure without special equipment. The Hardening Soil model do not account for this material behaviour. However, the Hardening Soil model with small-strain stiffness take the small-strain stiffness' non-linear dependency on strain amplitude properly into account (Brinkgreve et al., 2017).

The very small-strain stiffness of soils, G_0, can be determined from the in situ measurements of shear wave velocity, and the relationship in equation 5.1, where ρ is the soil density and v is the shear wave velocity. Andersen (1989) has determined the initial shear modulus for Baskarp sand by measuring shear wave velocity through triaxial specimens and found that $G_0 = 200$ MPa for tests with $\sigma'_v = 249.9$ kPa, $\sigma'_h = 112,7$ kPa and $e = 0.518$.

$$G_0 = \rho \times v^2 \tag{5.1}$$

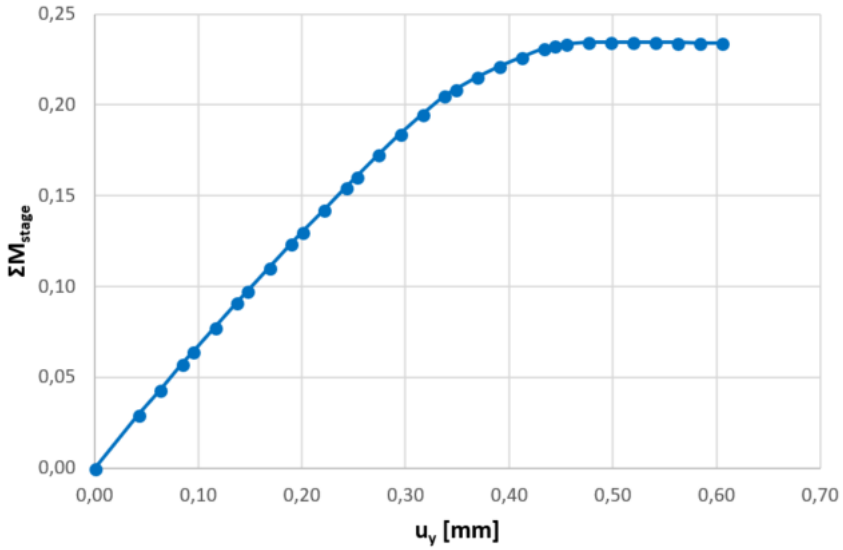

Figure 5.14: Drained pull-out capacity when an upward load of 150 kN/m is applied to the caisson skirt.

5.2.3 Extraction Resistance

Extraction resistance tests are performed in PLAXIS, and results from these tests are used to determine friction parameters of interfaces. The roughness of the interfaces is dependent on the strength reduction factor, R_{inter}. In addition will the interface friction angle, ϕ', affect the extraction resistance. By choosing $R_{inter} = 1$ and $\phi' = 20°$, which gives $R_{inter} \times \tan\phi = 0.37$, a drained extraction capacity of 15.7 kPa is found. This is very close to the capacity of 15 kPa from the drained extraction tests conducted in connection with the centrifuge tests described in section 4.4. The dilatancy angle is during these PLAXIS analyses set to $\psi = 0°$. Figure 5.14 shows a plot of the completed proportion of the plastic calculation, ΣM_{stage}, against vertical displacement of the caisson skirt, u_y. As an upward vertical load of 150 kN/m is applied at the top of the skirt, the capacity becomes $\frac{M_{stage} \times 150 \times 2\pi r}{\pi r^2}$, which for a caisson with radius $r = 4$ m is 15.7 kPa.

5.2.4 Consolidation Parameters

The enhanced gravity of the centrifuge experiments results in increased stresses, while the permeability remains unchanged. However, the dimensions in the model are scaled down with a

factor identical to the enhancement of the gravitational acceleration. This means that the time for consolidation to occur is different in the model and prototype. For both cases equation 5.2 from Terzaghi (1951) explains the relationship between time, soil volume and ability for fluid to run through the soil pores.

$$t = T_v \times \frac{h^2}{C_v} \tag{5.2}$$

h is the drainage path, T_v is the time factor and t is the time of consolidation. The coefficient of consolidation, C_v, is identical for the model and prototype when the same soil is used. T_v is dependent on normalised geometry and rate of drainage, and is consequently the same in the model and prototype. Hence, the drainage path, h, is the only factor to change in addition to the time.

The consolidation time for prototype and model is given in equation 5.3 and 5.4, respectively.

$$t_{prototype} = T_{v,prototype} \times \frac{h^2_{prototype}}{C_{v,prototype}} \tag{5.3}$$

$$t_{model} = T_{v,model} \times \frac{h^2_{model}}{C_{v,model}} \tag{5.4}$$

As the aim is to achieve the same degree of consolidation, T_v, equation 5.3 and 5.4 are used to find the relationship between the time in prototype and model given in equation 5.5.

$$\frac{t_{model}}{t_{prototype}} = \left(\frac{h_{model}}{h_{prototype}}\right)^2 = \frac{1}{\bar{N}^2} \tag{5.5}$$

Considering the suction caisson under investigation, $\bar{N} = 100$, which means that the whole model test must be performed $100^2 = 10000$ times faster than the prototype. This is in practice very hard to accomplish. A more viscous fluid is therefore added to the soil sample. For the samples with 100 cSt and 660 cSt pore fluid viscocity, the time to conduct the model tests is extended 100 and 660 times, respectively. For modeling purpose, the remaining time differ-

ence is accounted for by making the pore fluid dissipate faster as the permeability in the simulations is increased. The input value for permeability in PLAXIS has therefore changed from $k = 8.04 \times 10^{-5} m/s$ in the model experiments to $k = 8.04 \times 10^{-3}$ for test with 100 cSt pore fluid viscosity and $k = 0.53 \times 10^{-3}$ for tests with 660 cSt pore fluid viscosity.

5.2.5 Overview of Input Parameters and Description of Other Materials

An overview of the input parameters is given in table 5.3. The material denoted "best estimate" represents the material assumed to reproduce the centrifuge experiments most precisely based on the given data. The stiffness parameters for this material is based on the odometer test which parameters are given in table 5.2. In addition to the best estimate material, parameters of sands of different densities are given in the PLAXIS manual, and further used in the simulations (Brinkgreve et al., 2017). The parameters from these materials are also given in table 5.3. The permeability parameter, k, for all materials are based on the value found in section 5.2.4.

Table 5.3: Input parameters for materials used in PLAXIS simulations. The parameters for loose, dense and medium sand is found in the PLAXIS manual by Brinkgreve et al. (2017).

Parameter	Loose	Medium	Dense	Best estimate
E_{50}^{ref} $[kN/m^2]$ (for $p_{ref} = 100\ kN/m^2$)	20000	30000	40000	120000
E_{ur}^{ref} $[kN/m^2]$ (for $p_{ref} = 100\ kN/m^2$)	60000	90000	120000	500000
$E_{oed}^{ref}[kN/m^2]$ (for $p_{ref} = 100\ kN/m^2$	20000	30000	40000	110000
Cohesion c	0.0	0.0	0.0	0.0
Friction angle ϕ	30	35	40	44.5
Dilatancy angle ψ	0	5	10	24.2
Poisson's ration ν_{ur}	0.2	0.2 0.2	0.2	
Power m	0.5	0.5	0.5	0.25
K_0^{NC} (using cap)	0.5	0.43	0.36	0.45
Tensile strength $[kN/m^2]$	0.0	0.0	0.0	0.0
Failure ration	0.9	0.9	0.9	0.9
Permeability k $[m/s]$	8.04×10^{-3}	8.04×10^{-3}	8.04×10^{-3}	8.04×10^{-3}
Unsaturated unit weight γ_{unsat} $[kN/m^3]$	11	11	11	11
Saturated unit weight γ_{sat} $[kN/m^3]$	21	21	21	21

Chapter 6

Results

This chapter presents the results from the centrifuge experiments conducted at UWA and recalculation of the same experiments using PLAXIS. The results are further discussed in chapter 7.

6.1 Centrifuge Experiments

Chapter 4 describes the procedure and basic principles of the centrifuge experiments conducted at UWA. The applied loads from a test with different pore fluid viscosity, 100 cSt and 660 cSt (named test 4-2 and 6-1 in Bienen et al. (2018a)), and approximately similar cyclic loading is presented in table 6.1 and figure 6.1. The tests consist of four different load packets with constant load amplitude. The target mean stress is 8 kPa for all load packets, but the achieved value is slightly varying for the different load packets. Compression is defined positive and tension is negative. The results from these two experiments are further examined.

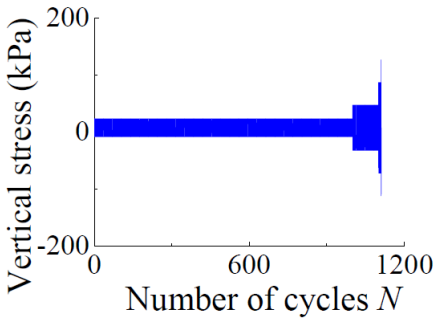

Figure 6.1: Icon illustrating loading history with cyclic amplitude, mean stress and number of cycles (Bienen et al., 2018a).

Table 6.1: The table illustrates what cyclic loading the sample has been exposed to (adapted from Bienen et al., 2018a).

Packet number	Number of of cycles, N	Achieved mean stress [kPa]	Achieved amplitude [kPa]
1	1000	9 (100 cSt) 8 (660 cSt)	±12 (100 cSt) ±14 (660 cSt)
2	100	12 (100 cSt) 9 (100 cSt)	±38 (100 cSt) ±38 (660 cSt)
3	10	10 (100 cSt) 9 (660 cSt)	±77 (100 cSt) ±77 (660 cSt)
4	1	8 (100 cSt) 9 (660 cSt)	±118 (100 cSt) ±116 (660 cSt)

6.1.1 Displacement

Each load cycle generates both cyclic and accumulated deformation. Parts of the cyclic displacement response for each packet are illustrated in figure 6.2 and 6.3 for experiments with pore fluid viscosity 100 cSt and 660 cSt, respectively. The displacement is presented in prototype scale, where settlement is positive and heave is negative.

The very first cycle of the time history starts at zero displacement. At this point the sample experienced mean load, which means that total permanent heave or settlement (accumulated displacement) of the caisson is measured from the mean point of the deformation cycle. At the end of the load sequence, the caisson has heaved for the two tests with different pore fluid viscosity. This can be seen by the negative value of the mean displacement after load packet 4 in figure 6.2 and 6.3. However, the same behaviour is not shown in all load packets. As an example, figure 6.4 illustrates a settlement of approximately 5 mm during package 2, while figure 6.5 shows a total heave of almost 40 mm in packet 3 for the test with pore fluid viscosity of 100 cSt.

As described in section 3.1.2, accumulated deformation may occur for structures that experience high cyclic loading. The effect of accumulated deformation, as sown in figures 6.4 and 6.5, can be further studied using the HCA model described in section 3.2. Due to time limitations in the project period of the master thesis, the study of the HCA model is limited to the theory part.

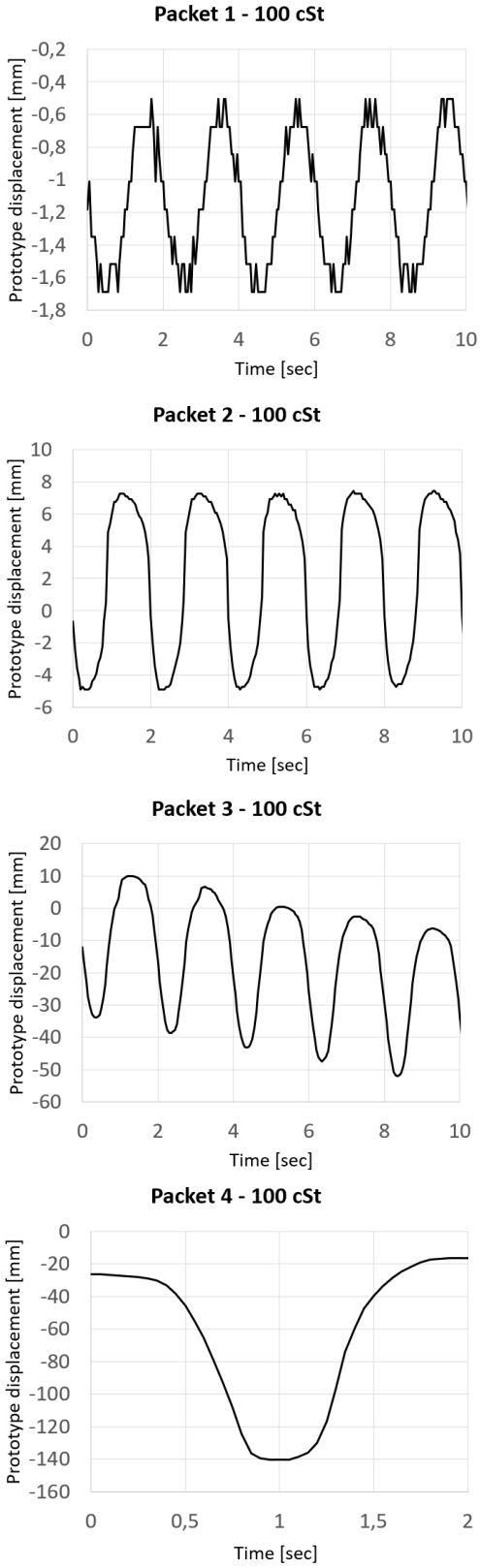

Figure 6.2: Time histories for centrifuge test with pore fluid viscosity 100 cSt. Note the different scales on the axes.

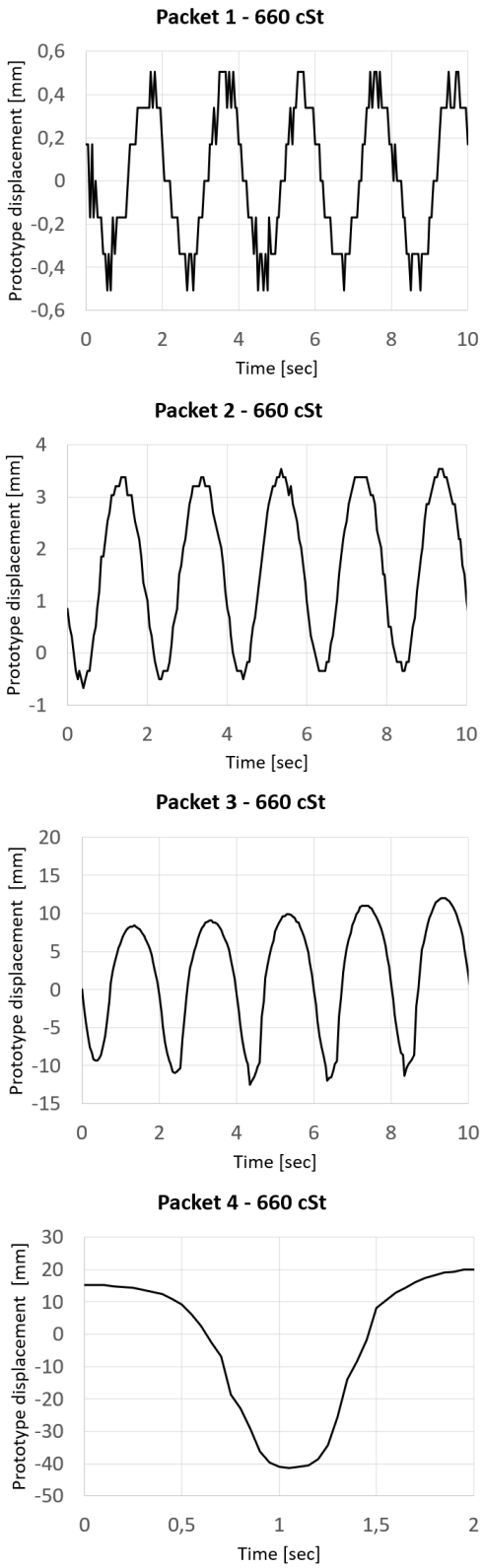

Figure 6.3: Time histories for centrifuge test with pore fluid viscosity 660 cSt cSt. Note the different scales on the axes.

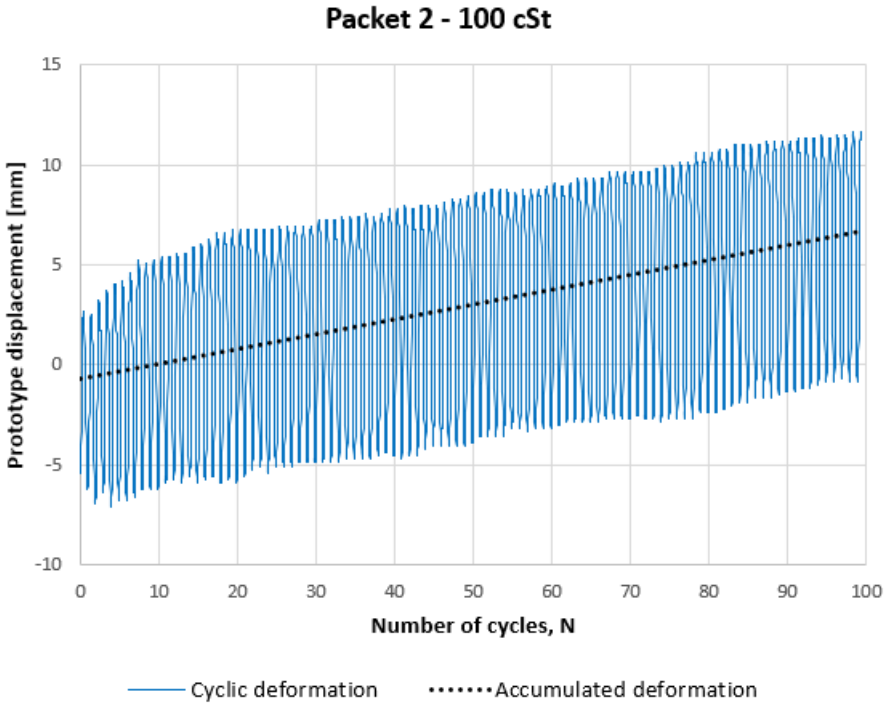

Figure 6.4: Accumulated deformation for packet 2 and pore fluid viscosity 100 cSt. The caisson is settling.

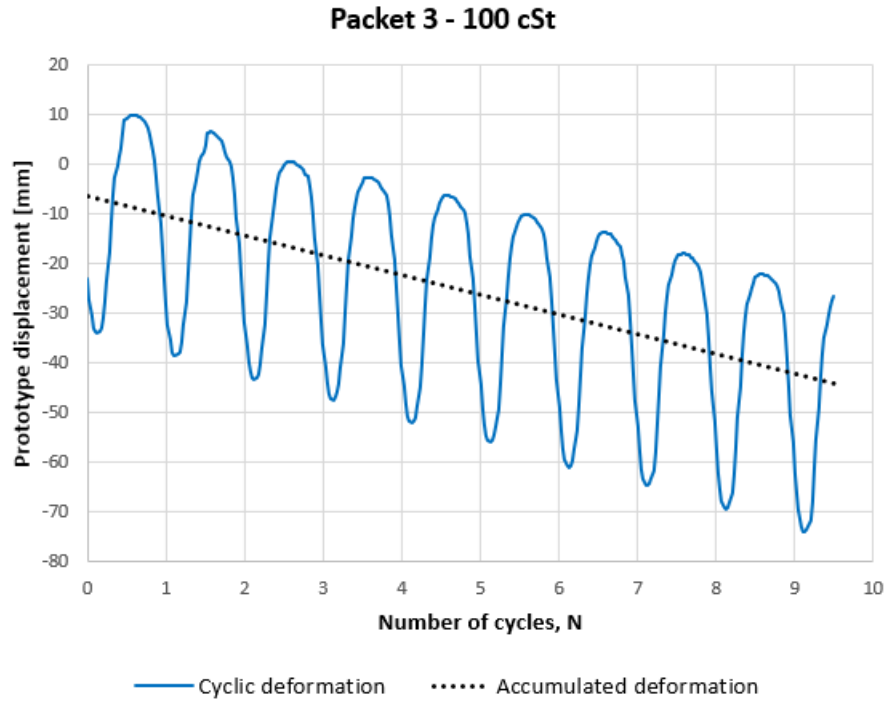

Figure 6.5: Accumulated deformation for packet 2 and pore fluid viscosity 100 cSt. The caisson is heaving.

6.1.2 Total Stress and Pore Pressure

Total stress and pore pressure are measured right beneath the caisson lid. Figure 6.6 shows results for tests with pore fluid viscosity 100 cSt, and figure 6.7 shows results for tests with pore fluid viscosity of 660 cSt. The start mean values for both total stress and pore pressure is zero. This means that any stress in the soil prior to the cyclic loading is unknown.

The results show that the curves for total stress and pore pressure are almost equal. This means that approximately all changes in total stress at the measuring point is due to pore pressure changes. However, the deformation for experiments with pore fluid viscosity 100 cSt is bigger than experiments with 660 cSt. This may indicate that the soil does not behave fully undrained and that consolidation parameters are of importance.

6.1.3 Amplitudes of Cyclic Applied Load, Displacement, Total Stress and Pore Pressure

Figure 6.8 illustrates how the peak of the cyclic amplitude of displacement, total stress and pore pressure changes with the peak of applied stress, both for tests with pore fluid viscosity 100 cSt and 660 cSt. The applied stress on the vertical axis is the peak value of maximum applied stress in tension or compression measured from mean stress level. The displacement, total stress and pore pressure on the horizontal axis are the magnitude of the cyclic amplitude in either tension or compression measured from the same spot where the mean stress level of applied stress occur. If a phase difference is present, the curve is shifted so the peaks are on the same spot.

The figures show that in general the amplitudes in tension are bigger than the amplitude in compression. The difference becomes bigger as the applied stress amplitude increases. For packet 1 and 2 many of the values are almost equal. The amplitudes shown in figure 6.8 are summarised in table 6.2 and 6.3.

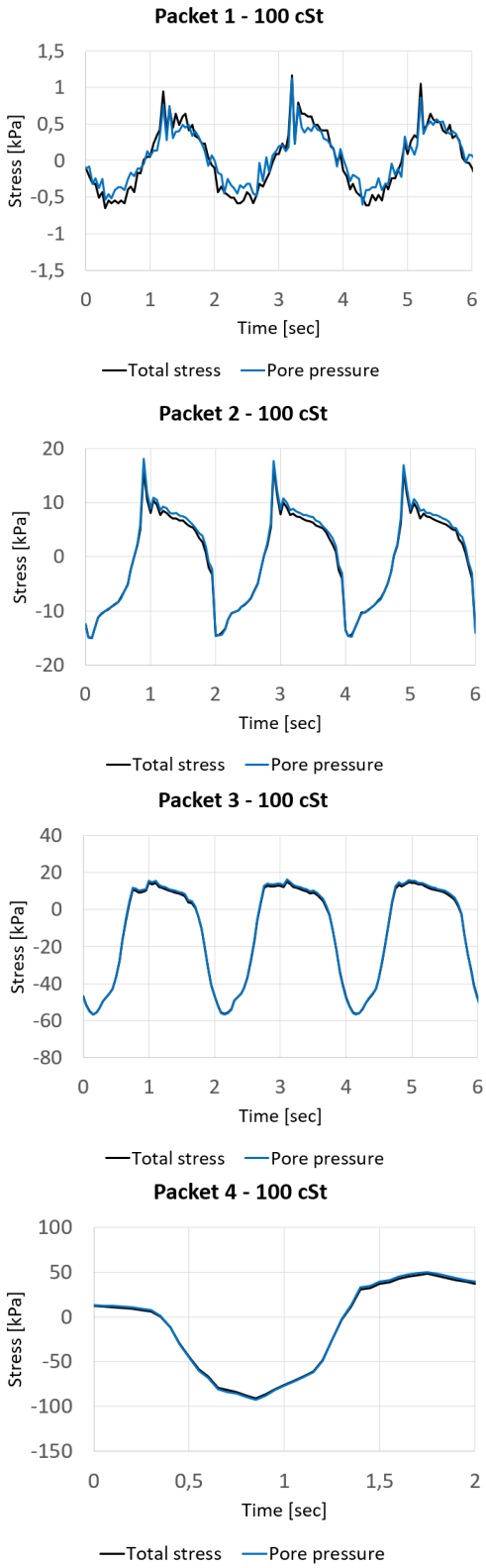

Figure 6.6: Total stress and pore pressure for centrifuge test with pore fluid viscosity 100 cSt. Note the different scales on the axes.

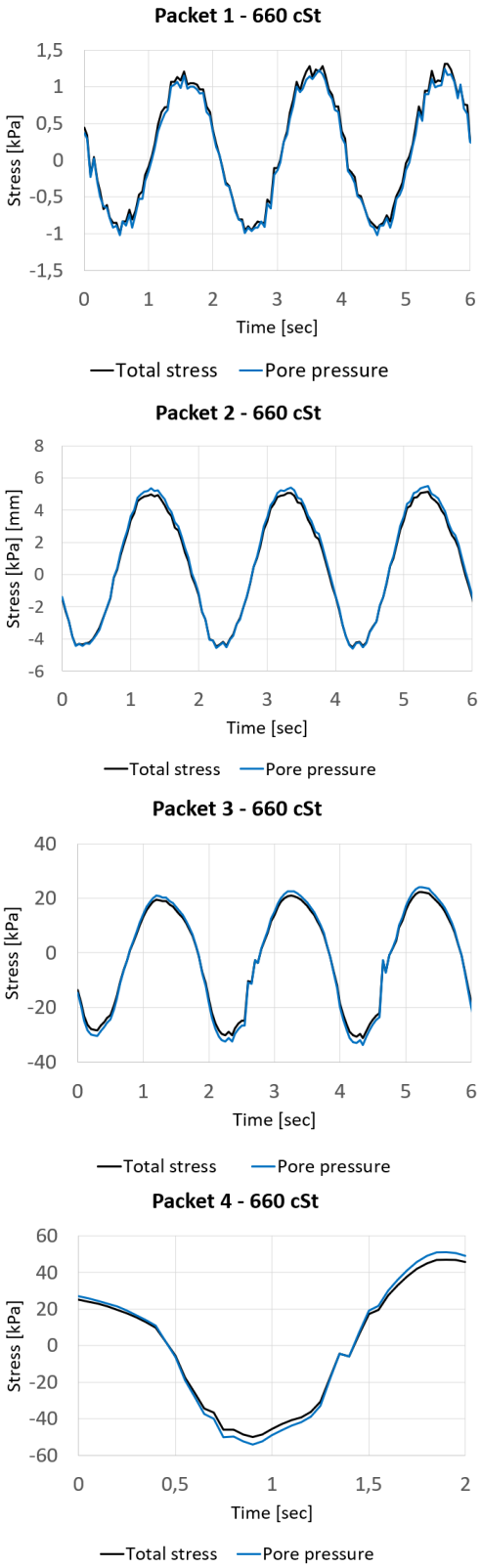

Figure 6.7: Total stress and pore pressure for centrifuge test with pore fluid viscosity 660 cSt. Note the different scales on the axes.

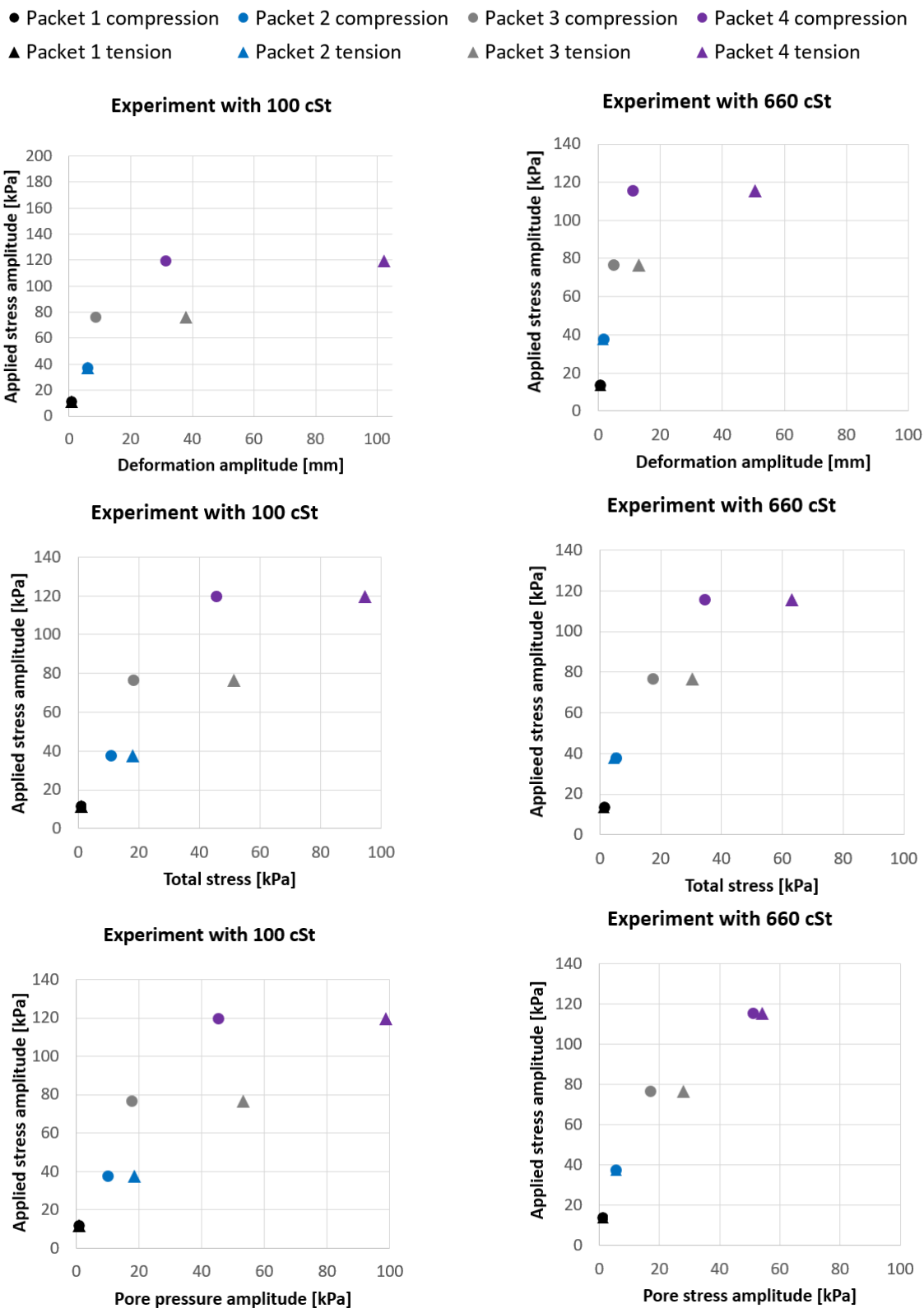

Figure 6.8: Peak amplitudes of cyclic deformation, total stress and pore pressure for conducted experiments.

Table 6.2: Magnitude of cyclic deformation amplitude, total stress amplitude and pore pressure in compression and tension for different load packets. The experiments are performed with fluid viscosity of 100 cSt.

Experiment with 100 cSt

Packet number	Type of load	Deformation amplitude [mm]	Total stress [kPa]	Pore pressure [kPa]
1	Compression	0.7	0.6	0.6
	Tension	0.7	0.6	0.6
2	Compression	5.7	10.5	9.7
	Tension	5.7	17.7	18.2
3	Compression	8.4	18.0	17.4
	Tension	37.6	51.1	53.0
4	Compression	31.1	45.4	45.1
	Tension	101.9	94.3	98.6

Table 6.3: Magnitude of cyclic deformation amplitude, total stress amplitude and pore pressure in compression and tension for different load packets. The experiments are performed with fluid viscosity of 660 cSt.

Experiment with 660 cSt

Packet number	Type of load	Deformation amplitude [mm]	Total stress [kPa]	Pore pressure [kPa]
1	Compression	0.5	1.1	0.9
	Tension	0.4	1.0	0.8
2	Compression	1.5	4.9	5.2
	Tension	1.3	4.3	4.3
3	Compression	6.3	16.7	17.2
	Tension	22.8	27.7	30.1
4	Compression	10.9	34.3	51.0
	Tension	50.3	62.7	54.0

6.2 Recalculation Using PLAXIS

The centrifuge experiment with cyclic loading as in figure 6.1 is recalculated using PLAXIS. Different calculation types are used to understand how the model works. The simulations are preformed as plastic analyses, either fully drained or fully undrained, or as consolidation analyses where the cyclic load is applied with a frequency of 0.5 Hz, similar to the centrifuge experiments.

The material adapted to the oedometer test, which stiffness parameters are shown in table 5.2, is considered as a best estimate material. The materials with different densities, presented in table 5.3, are also used in the simulations.

Figures for cyclic peak amplitudes for displacements, total stress and pore pressures in PLAXIS simulations are presented. This corresponds to the peak amplitudes shown in figure 6.8 for centrifuge tests. Figure 6.9 presents results from simulations using best estimate sand, figure 6.10 presents results from dense sand, figure 6.11 presents results from medium dense sand and 6.12 presents results from loose sand. Table 6.4 summarises the values in figure 6.9 to 6.12.

The results show the same pattern as can be seen for the centrifuge experiments, with bigger amplitudes in tension than in compression, and a difference between compression and tension which becomes larger with the applied stress amplitude.

As the model in PLAXIS goes to failure when loaded to packet 4, no results of PLAXIS simulations from this packet is presented. This also applies to the fully undrained calculations in packet 3 for loose sand.

A comparison of the results from centrifuge tests and PLAXIS simulations is presented for peak amplitude displacements in figure 6.13, total stress in figure 6.14 and pore pressure in figure 6.15. In general, the deformation is underestimated and the total stress and pore pressure are overestimated in the PLAXIS simulations.

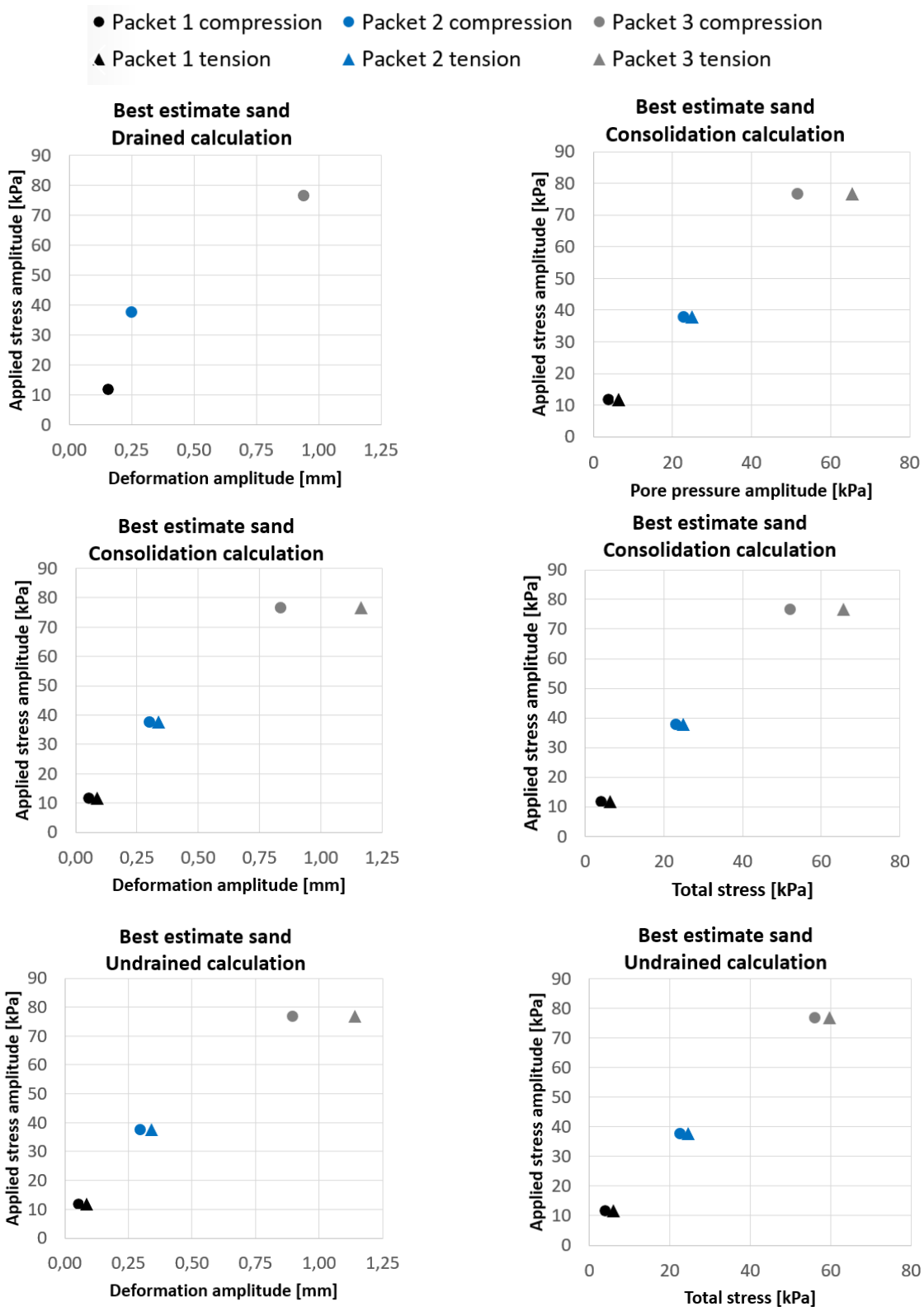

Figure 6.9: Peak amplitudes of cyclic deformation, total stress and pore pressure for calculations in PLAXIS using the best estimate sand.

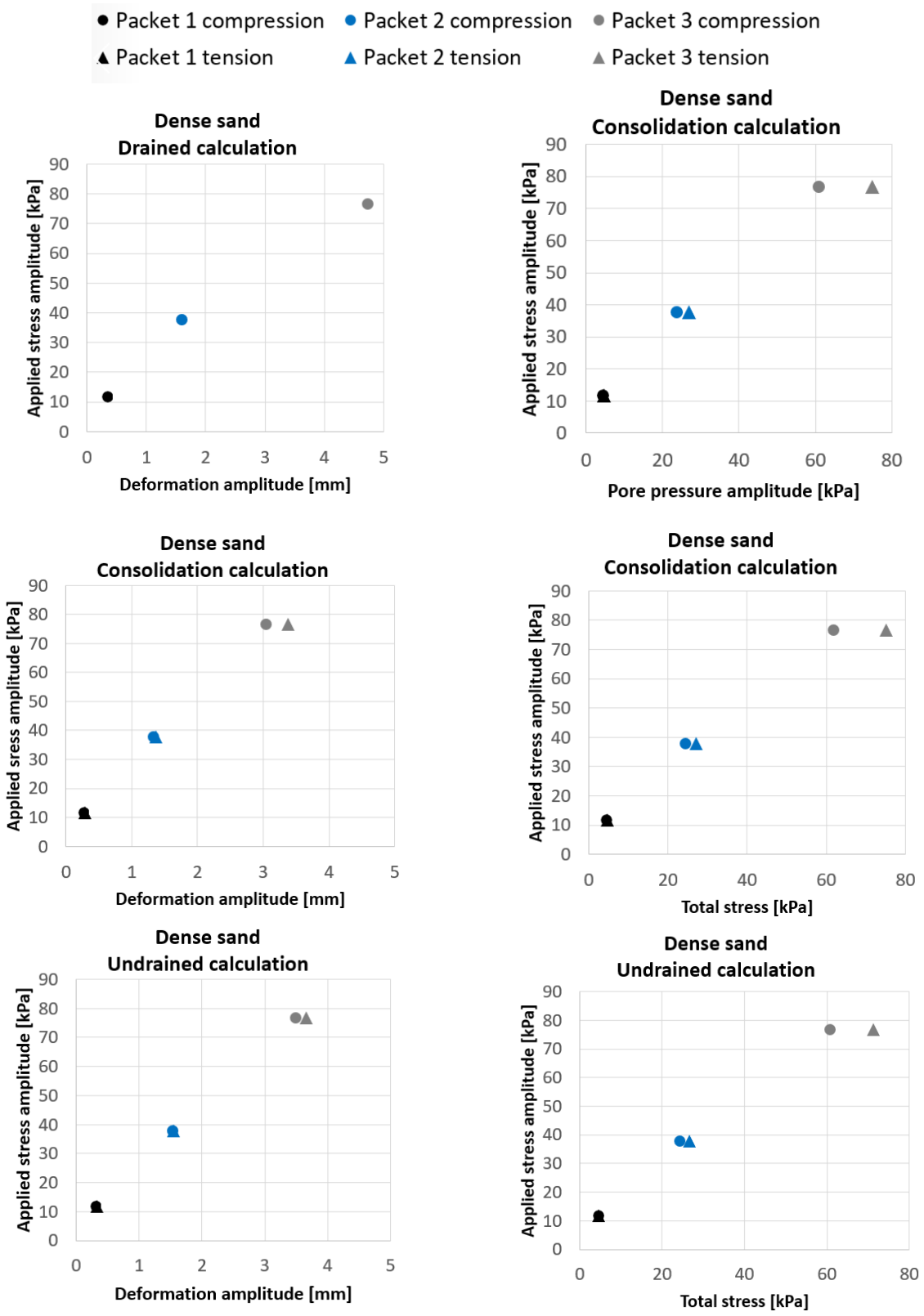

Figure 6.10: Peak amplitudes of cyclic deformation, total stress and pore pressure for calculations in PLAXIS using dense sand.

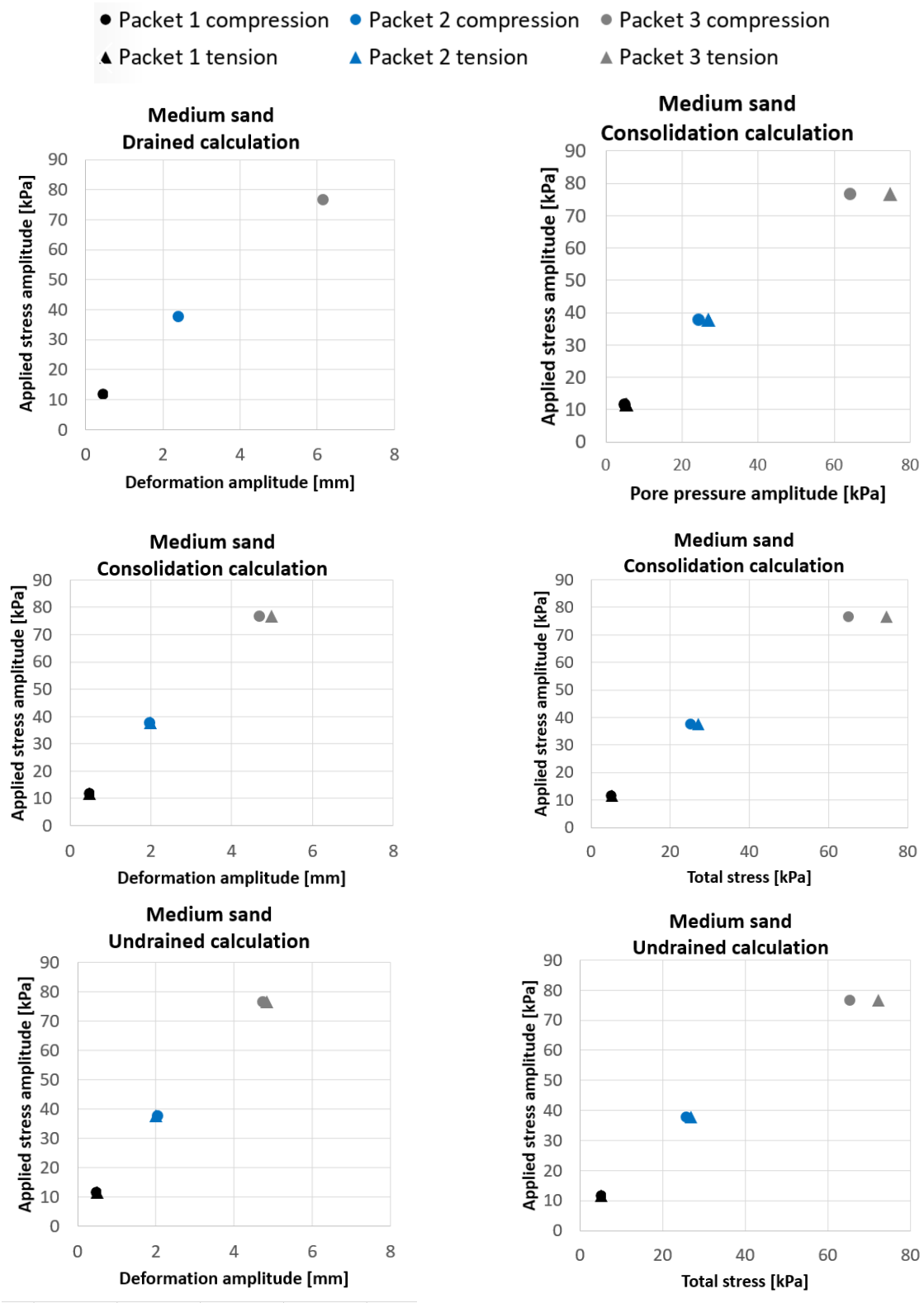

Figure 6.11: Peak amplitudes of cyclic deformation, total stress and pore pressure for calculations in PLAXIS using medium dense sand.

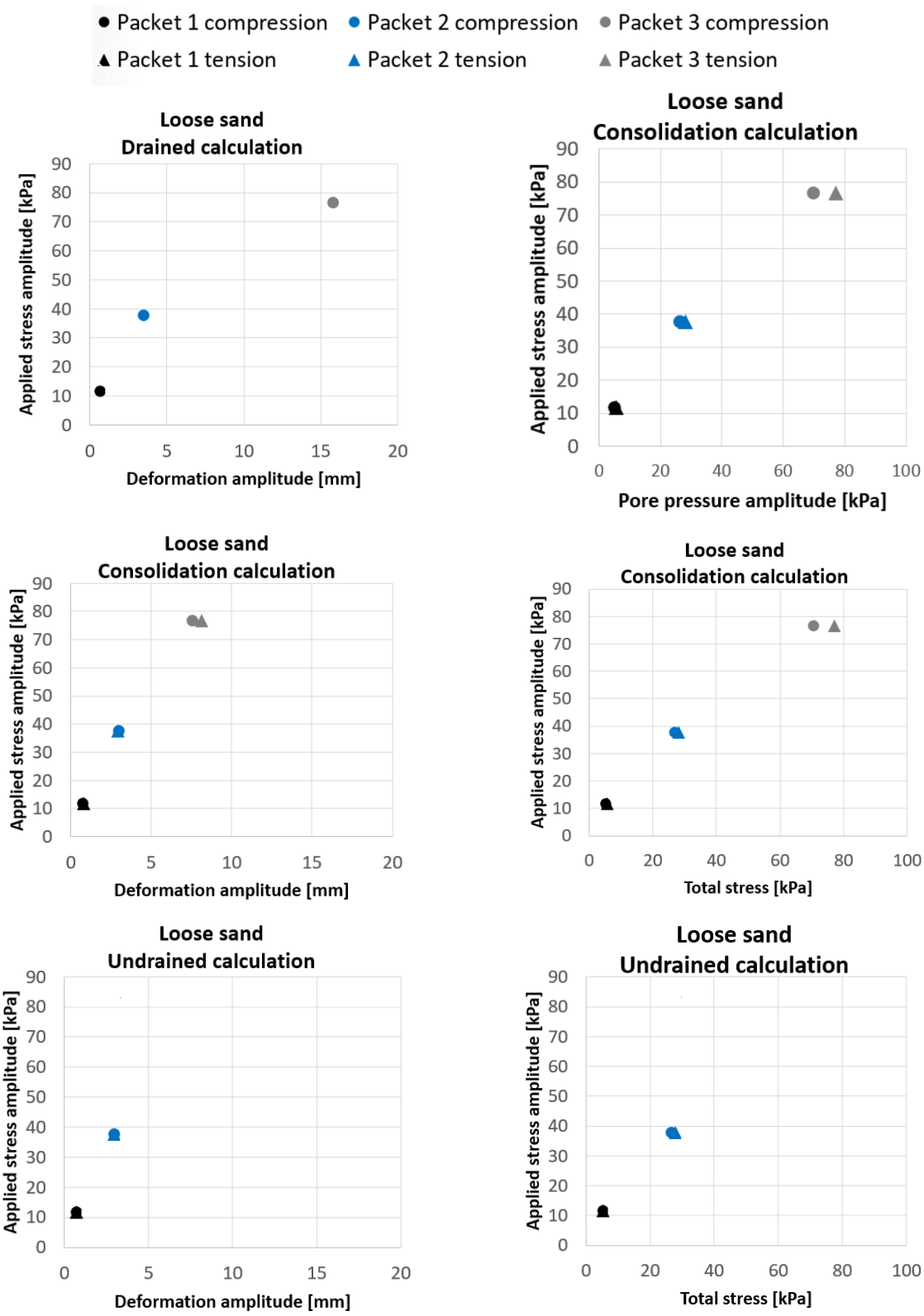

Figure 6.12: Peak amplitudes of cyclic deformation, total stress and pore pressure for calculations in PLAXIS using loose sand.

Table 6.4: The table shows a summary of peak deformation, total stress and pore pressure amplitudes for simulations made in PLAXIS in addition to centrifuge tests (centrif. test).

			Deformation amplitude [kPa]				Total stress amplitude [kPa]			Excess pore pressure amplitude [kPa]		
Packet number	Type of material	Type of load	Undrained calc.	Cons. calc.	Drained calc.	Centrif. test	Undrained calc.	Cons. calc.	Centrif. test	Undrained calc.	Cons. calc.	Centrif. test
1	Best estimate	Compression	0.05	0.05	0.15	-	3.75	3.81	-	3.54	3.61	-
		Tension	0.08	0.08	-	-	5.84	6.03	-	5.84	6.03	-
	Dense	Compression	0.30	0.26	0.33	-	4.30	4.20	-	4.15	4.11	-
		Tension	0.31	0.28	-	-	4.40	4.44	-	4.40	4.38	-
	Medium	Compression	0.46	0.46	0.43	-	4.99	4.95	-	4.81	4.78	-
		Tension	0.47	0.47	-	-	5.04	5.09	-	5.04	5.06	-
	Loose	Compression	0.66	0.71	0.63	-	4.93	4.92	-	4.77	4.75	-
		Tension	0.68	0.72	-	-	4.99	5.38	-	5.00	5.34	-
	100 cSt	Compression	-	-	-	0.7	-	-	0.6	-	-	0.6
		Tension	-	-	-	0.7	-	-	0.6	-	-	0.6
	660 cSt	Compression	-	-	-	0.5	-	-	1.1	-	-	0.9
		Tension	-	-	-	0.4	-	-	1.0	-	-	0.8
2	Best estimate	Compression	0.29	0.30	0.24	-	22.36	22.83	-	22.16	22.65	-
		Tension	0.34	0.34	-	-	24.46	24.77	-	24.48	24.80	-
	Dense	Compression	1.52	1.31	1.58	-	24.13	24.15	-	23.46	23.50	-
		Tension	1.53	1.36	-	-	26.35	26.87	-	26.22	26.75	-
	Medium	Compression	2.02	1.94	2.37	-	25.52	24.85	-	24.95	24.19	-
		Tension	1.98	1.97	-	-	26.78	26.84	-	26.95	26.67	-
	Loose	Compression	2.91	2.92	3.45	-	26.25	26.56	-	25.73	26.08	-
		Tension	2.90	2.89	-	-	27.74	27.91	-	26.46	27.67	-
	100 cSt	Compression	-	-	-	5.7	-	-	10.5	-	-	9.7
		Tension	-	-	-	5.7	-	-	17.7	-	-	18.2
	660 cSt	Compression	-	-	-	1.5	-	-	4.9	-	-	5.2
		Tension	-	-	-	1.3	-	-	4.3	-	-	4.3
3	Best estimate	Compression	0.89	0.83	0.94	-	55.89	51.79	-	55.37	51.30	-
		Tension	1.14	1.16	-	-	59.51	65.48	-	59.17	65.32	-
	Dense	Compression	3.48	3.03	4.72	-	60.54	61.61	-	59.44	60.58	-
		Tension	3.64	3.37	-	-	71.11	74.90	-	70.78	74.60	-
	Medium	Compression	4.72	4.67	6.13	-	65.12	64.82	-	64.17	63.93	-
		Tension	4.83	4,97	-	-	72.05	74.49	-	71.92	74.34	-
	Loose	Compression	-	7.52	15.72	-	-	70.37	-	-	69.36	-
		Tension	-	8.05	-	-	-	76.73	-	-	76.75	-
	100 cSt	Compression	-	-	-	8.4	-	-	18.0	-	-	17.4
		Tension	-	-	-	37.6	-	-	51.1	-	-	53.0
	660 cSt	Compression	-	-	-	6.3	-	-	16.7	-	-	17.2
		Tension	-	-	-	22.8	-	-	27.7	-	-	30.1

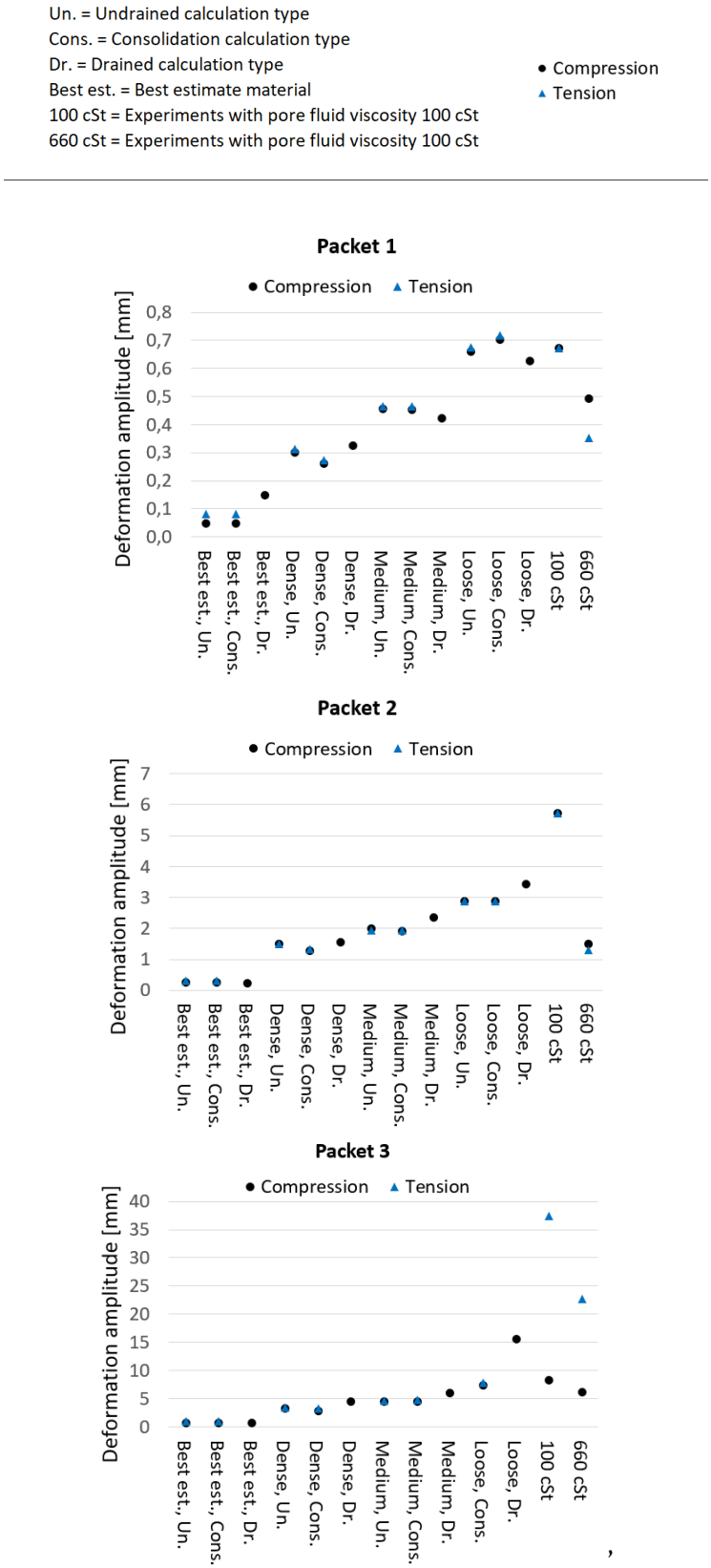

Figure 6.13: A summary of the peak deformation amplitudes from centrifuge tests and simulations in PLAXIS.

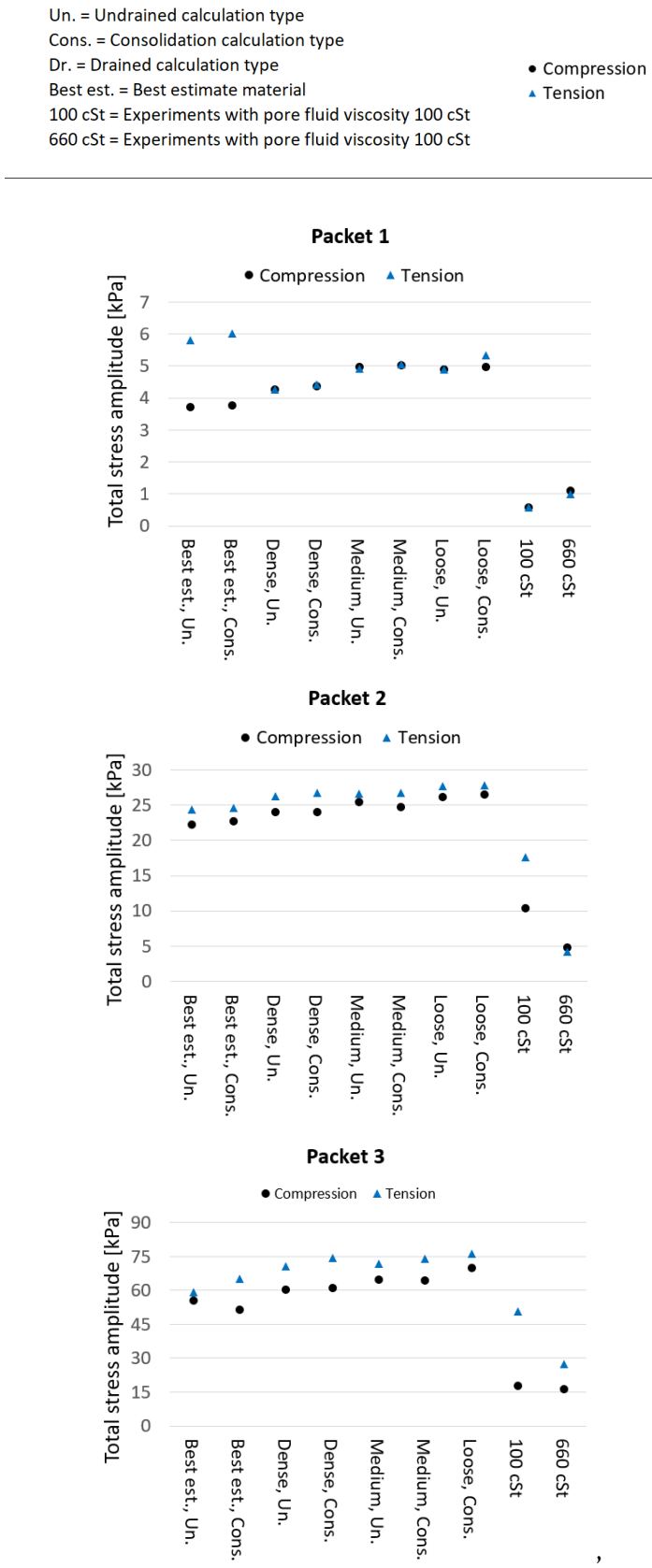

Figure 6.14: A summary of the peak total stress amplitudes from centrifuge tests and simulations in PLAXIS.

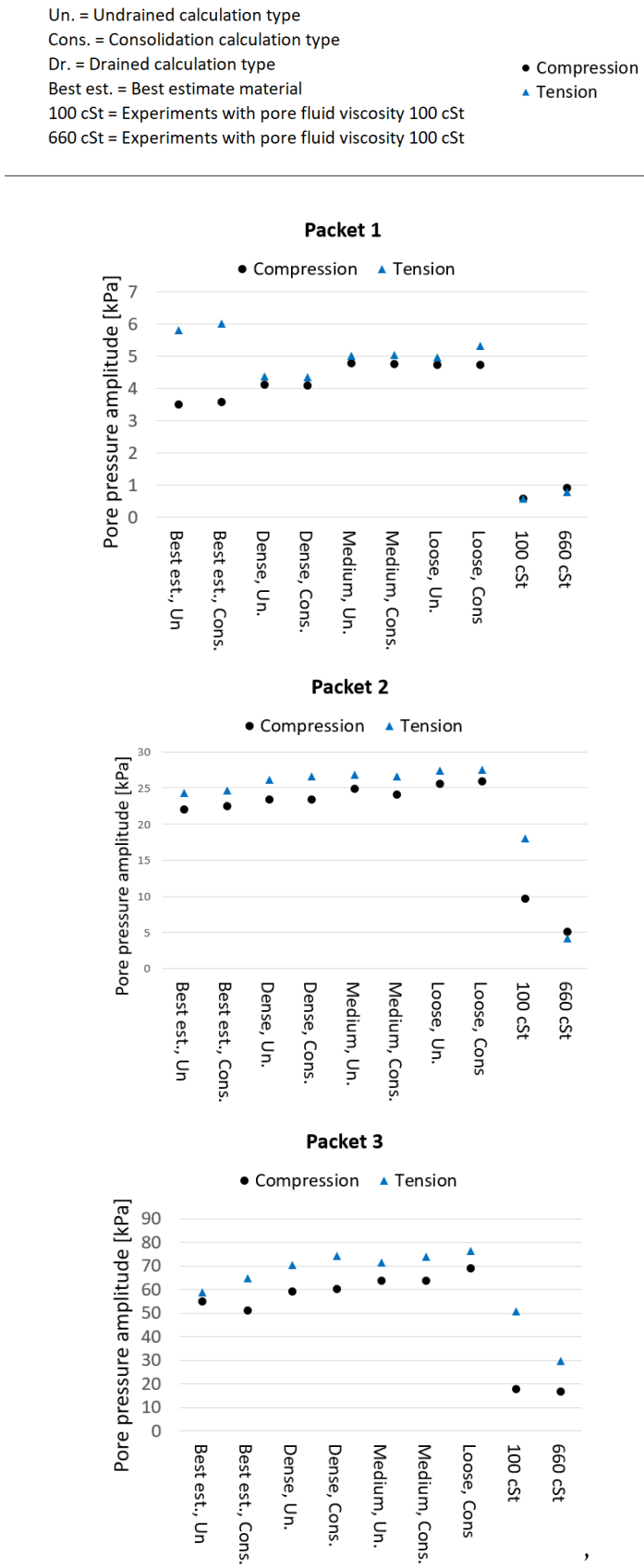

Figure 6.15: A summary of the peak pore pressure amplitudes from centrifuge tests and simulations in PLAXIS.

6.3 Miscellaneous Variations for PLAXIS Simulations

6.3.1 Replaced Soil Tip

For simulations with best estimate sand, a soil cluster around the soil tip has been replaced by the loose material. This is to account for different soil behaviours at different parts of the soil. The soil is exposed to load packet 2 and 3, and the calculation type in PLAXIS is consolidation calculation. The displacements from this calculations are shown in table 6.5, together with results in which the whole soil consists of best estimate or loose sand. The loose material around soil tip results in larger displacements. However, the enlargement of displacements are small compared to replacing the whole soil area with loose sand.

Table 6.5: Displacements for best estimate and loose sand in addition to a simulation of best estimate sand where the soil around the skirt tip has been replaced by loose sand. The consolidation calculation type is used. Results from centrifuge experiments are included for comparison.

Packet number	Type of material	Deformation [mm]	
		Compression	Tension
2	Best estimate sand	0.30	0.34
	Best estimate sand, soil tip replaced with loose sand	0.41	0.45
	Loose sand	2.90	2.89
	Centrifuge experiment 100 cSt	5.7	5.7
	Centrifuge experiment 660 cSt	1.5	1.3
3	Best estimate sand	0.83	1.16
	Best estimate sand, soil tip replaced with loose sand	1.09	1.26
	Loose sand	7.52	8.05
	Centrifuge experiment 100 cSt	8.4	37.6
	Centrifuge experiment 660 cSt	6.3	22.5

6.3.2 Variation in Permeability

The permeability is an important parameter in the calculations. To understand how the permeability parameter influences the results, simulations for loose sand exposed to load packet 2 have been conducted with different permeability parameters. Table 6.6 shows increasing displacement with permeability.

Table 6.6: The dependency of displacement, total stress and pore pressure amplitude on permeability for loose sand exposed to load packet 2. Results from centrifuge experiments subjected to the similar load packet are included for comparison.

PLAXIS simulations

Permeability $[m/s]$	Load direction	Displacement $[mm]$	Total stress $[kPa]$	Pore pressure $[kPa]$
8.04×10^{-3}	Compression	2.92	26.56	26.08
	Tension	2.89	27.91	27.67
8.04×10^{-2}	Compression	3.08	27.68	27.10
	Tension	2.90	28.00	27.80
8.04×10^{-1}	Compression	3.20	28.52	27.91
	Tension	2.93	28.52	28.40
8.04×10^{0}	Compression	3.53	29.96	29.20
	Tension	3.04	29.42	29.42
8.04×10^{1}	Compression	4.03	27.91	27.33
	Tension	3.45	29.59	29.54
8.04×10^{2}	Compression	5.29	17.54	12.44
	Tension	5.43	21.12	18.59
8.04×10^{3}	Compression	6.41	14.36	2.36
	Tension	14.55	26.74	20.20

Centrifuge experiments

Pore fluid viscosity $[cSt]$	Load direction	Displacement $[mm]$	Total stress $[kPa]$	Pore pressure $[kPa]$
100	Compression	5.7	10.5	9.7
	Tension	5.7	17.7	18.2
660	Compression	1.5	4.9	5.2
	Tension	1.3	4.3	4.3

6.3.3 Water Pocket Beneath Caisson Lid

To account for a possible gap between the caisson lid and soil, a thin soil layer right below the lid, is given softer soil properties. Simulations are conducted by initially using loose sand and apply load packet 2. The displacements in addition to stiffness parameters of the replaced thin layer are presented in table 6.7 and illustrate that this layer influences the displacements, especially in tension.

Table 6.7: Displacements for simulations using loose sand applied to load packet 2 performed with a small layer of softer soil beneath the caisson lid. Results from centrifuge experiments subjected to the similar load packet are included for comparison.

PLAXIS simulations					
Stiffness parameters				Displacements	
E_{50}^{ref} $[kPa]$	E_{oed}^{ref} $[kPa]$	E_{ur}^{ref} $[kPa]$	m $[-]$	Compression $[mm]$	Tension $[mm]$
50	50	150	0.5	4.42	3.20
30	30	90	0.5	4.26	6.02
10	10	30	0.5	4.53	12.19
Centrifuge experiments					
Pore fluid viscosity				Displacements	
100 cSt				5.7	5.7
660 cSt				1.5	1.3

Chapter 7

Discussion

In the following chapter the results from chapter 6 will be discussed. Firstly, cyclic peak amplitudes, including results from centrifuge experiments and simulations will be considered, followed by examination of the type of behaviour and choice of material. Finally, the reasons for difference in response in centrifuge experiments and PLAXIS simulations are discussed, hereunder loosening of soil due to installation, consolidation and redistribution of forces, gap between caisson lid and soil in addition to air bubbles in the pore fluid.

7.1 Discussion on Cyclic Peak Amplitudes

This section presents a discussion on the cyclic peak amplitudes from centrifuge experiments and PLAXIS simulations.

7.1.1 Centrifuge Experiments

The cyclic peak amplitudes from centrifuge experiments shown in figure 6.8 reveal that the deformation amplitudes increase non-linearly with applied stress amplitude. To emphasise the non-linear behaviour, examples of regression lines are added to the results in figure 7.1. As can

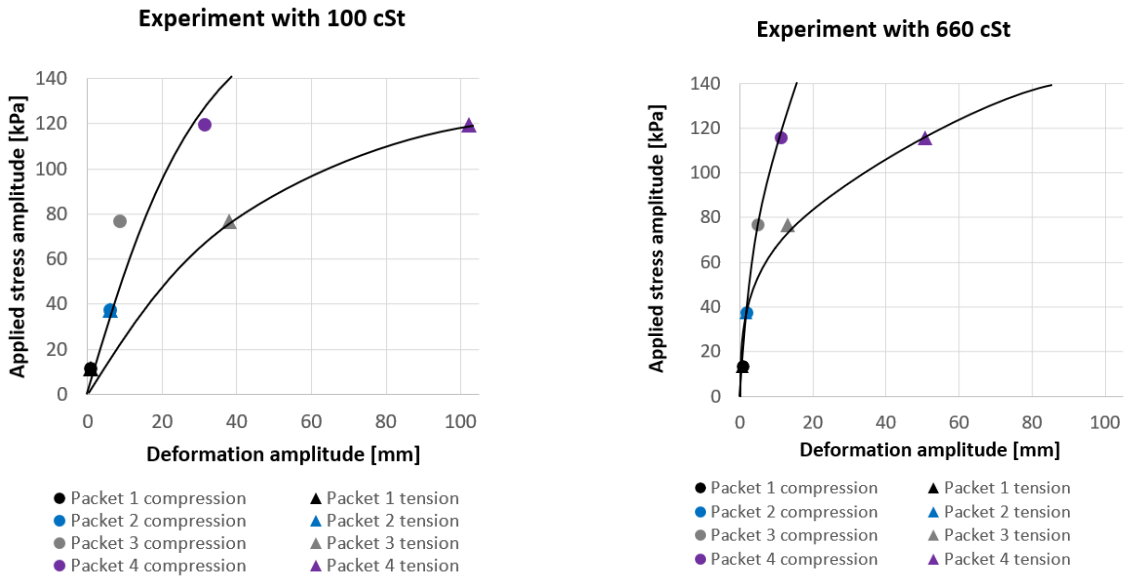

Figure 7.1: Peak deformation amplitudes with examples of regression lines for centrifuge experiments.

be seen from this figure, the regression lines are intersecting the origin, which is reasonable as the deformation amplitude should be zero as the load approaches zero.

When the load is increased to values of load packet 3 and 4, the curves show a clear difference in peak deformation amplitudes for compression and tension loading. A reason may be, as mentioned in section 3.1.1, that the soil is softer when the caisson is pulled up compared to pushed down. The soil stiffness is assumed to be non-linear, and gradually reduced towards the soil strength. The strength is effective stress-dependent and increases with the effective stresses. For drained and partly drained conditions, the effective stresses will, as described in section 3.1, increase under compressive loads and be reduced under tensile loads. Hence, the soil strength and stiffness reduce when the caisson is pulled up. For load packet 1 and 2, the behaviour in compression and tension is more equal as the applied loads are far form the maximum load capacity in both directions.

As can be seen from figure 6.13 and figure 7.1, the displacement is in general larger for lower pore fluid viscosity. This is expected as the consolidation is slower for lower permeability. When the load changes rapidly, the soil does not have time to consolidate before the direction of the load has changed.

Figure 6.8 also shows peak amplitudes for total stresses. For an assumed linear behaviour, the corresponding regression lines are drawn in figure 7.2. However, the regression lines intersect the negative part of the horizontal axis. By fully trusting these lines, a state with no applied load will result in tension forces in the soil, which is highly unrealistic.

By accounting for an offset in the measured data due to wrong calibration of the instruments or misinterpretation of the data, all the data points may be displaced parallel to make the regression line intersect the origin. This is shown in figure 7.3.

However, the relationship between applied load and total stress response is not necessarily proportional. From figure 7.4 one can assume that the data points fit more accurately a non-linear regression curve which actually intercepts the origin. Points deviating from the regression curves can be due to uncertainties in recordings of the stress, difference in distribution of forces for various load packages or inaccurate regression lines.

In addition to peak displacement and total stress amplitudes, figure 6.8 shows peak pore pressure amplitudes. Similar to the results for total stress, a non-linear regression line describes the behaviour of the pore pressure well. In addition, it is worth noting that the magnitudes of the pore pressure amplitudes and total stress amplitudes are very close to each other, as presented in table 6.2 and 6.3.

Another characteristic of the peak pore pressure amplitudes is the decreased pore pressure amplitude with increased pore fluid viscosity for tensile loading. This is the opposite of what is expected in many cases. A possible explanation for this strange behaviour is based on the ability to transfer forces to the skirt tip of the caisson. During fully drained extraction, the skirt tip has close to no capacity. However, as the pore fluid viscosity increases, the permeability is reduced, and the soil will approach an undrained behaviour. The undrained behaviour makes the skirt tip able to carry more loads, and a transfer of forces from the area around the caisson lid to the skirt tip possible. Hence, the pore pressure in the top of the caisson is reduced.

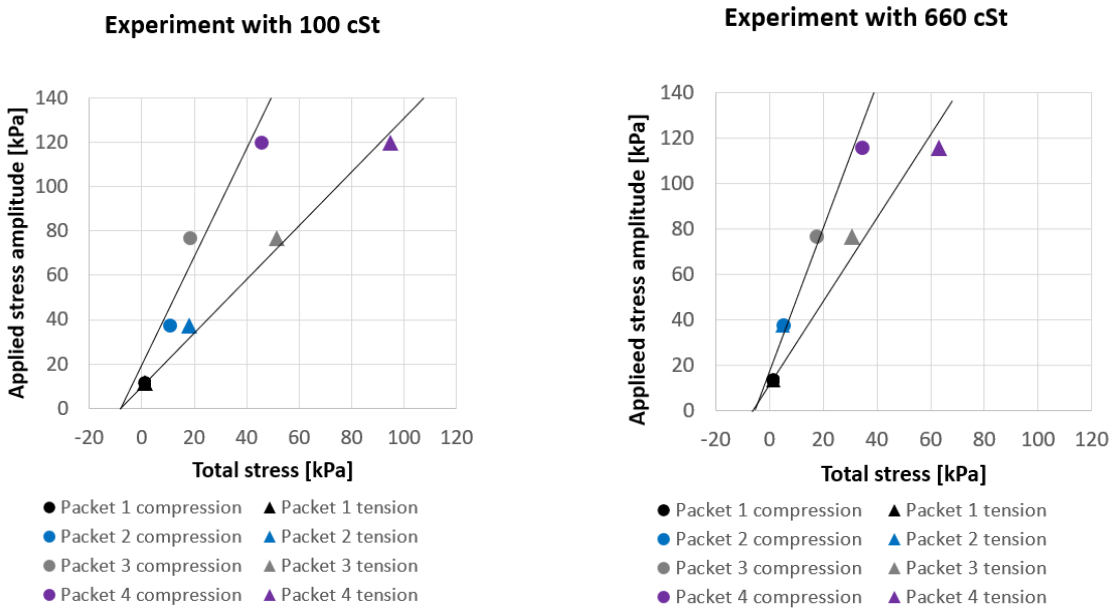

Figure 7.2: Peak total stress amplitudes with example of linear regression lines for centrifuge experiments.

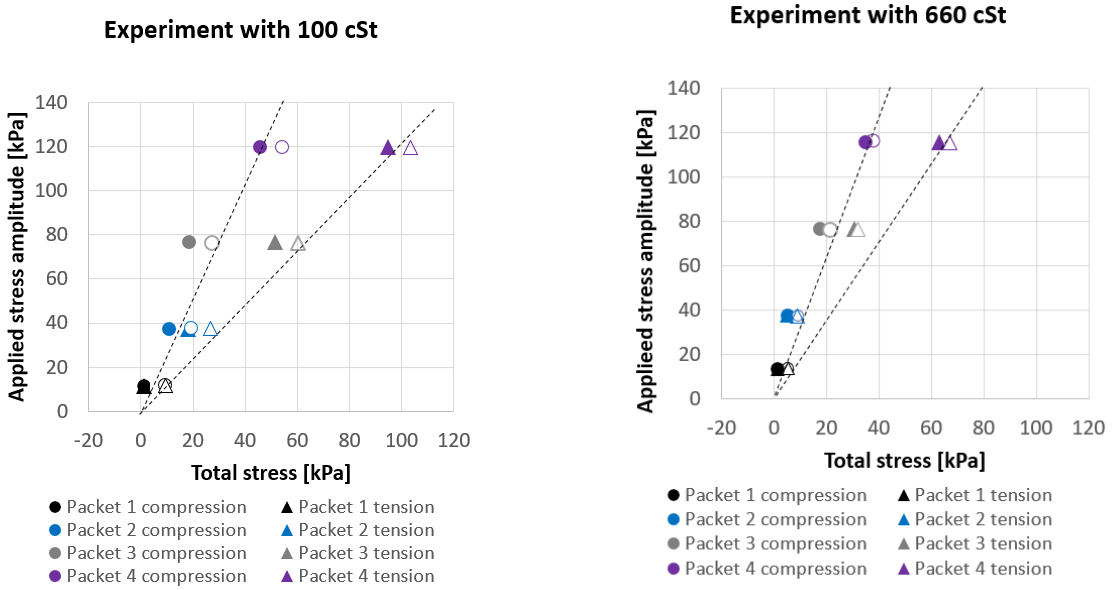

Figure 7.3: Peak total stress amplitudes with example of parallel displacement of the measured values from centrifuge experiments, and regression lines for the offset values. The points without shaded area represent offset values.

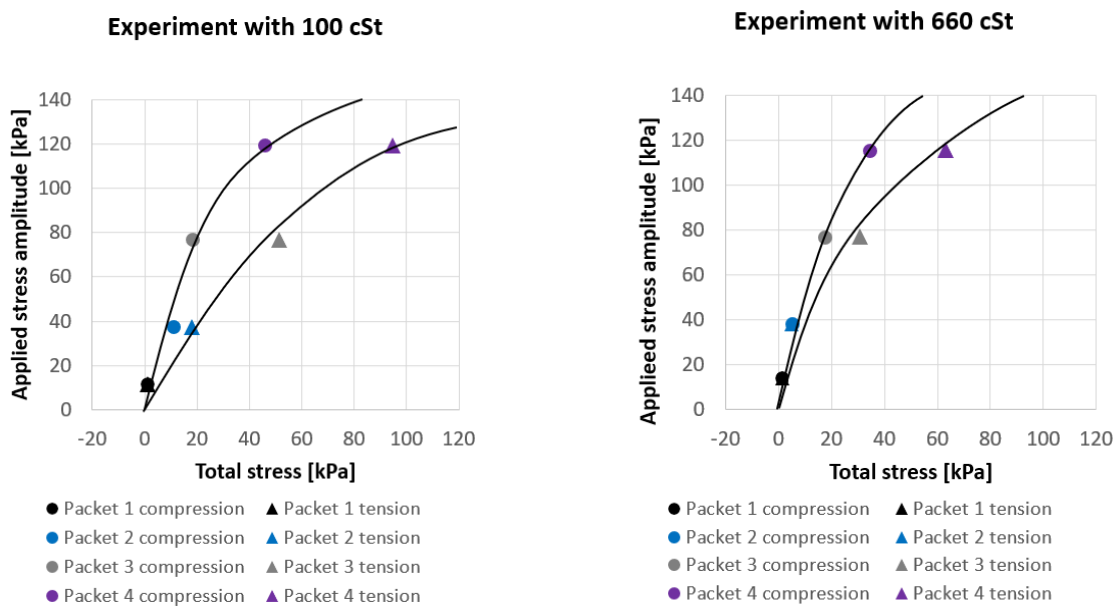

Figure 7.4: Peak total stress amplitudes with example of non-linear regression lines for centrifuge experiments.

7.1.2 PLAXIS Simulations

Figure 6.9 to 6.12 illustrate peak displacement, total stress and pore pressure amplitudes against applied stress amplitudes for different types of PLAXIS calculations and materials. Figure 6.13 to 6.15 show a summary of the amplitudes for different load packets.

The peak amplitudes from the displacement calculations show, when plotted against applied stress amplitude, a non-linear behaviour, with regression lines intersecting the origin. Consolidation calculations for loose sand show an example of this behaviour, which is illustrated in figure 7.5.

The summary of displacement amplitudes in figure 6.13 shows that the displacement in general is underestimated compared to the centrifuge experiments with pore fluid viscosity 100 cSt. The material which estimates the large displacements most accurately is the loose material. This material is very close to the displacements of load packet 1 in the centrifuge experiments but underestimates the displacements in load packet 2 and 3. The underestimation of displacements is discussed in more detail in section 7.3.

The figure also shows that the big difference between tension and compression is not very

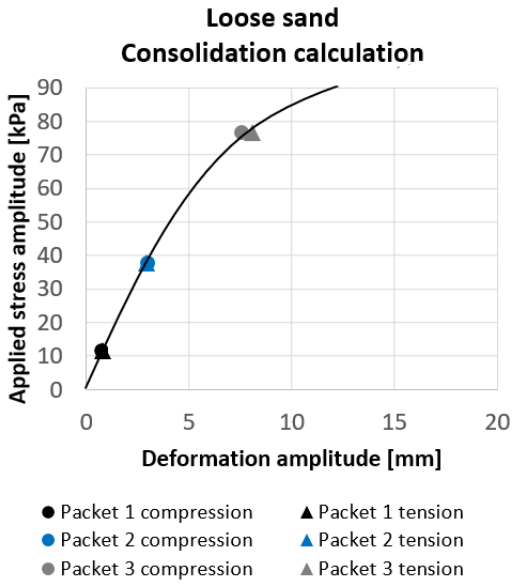

Figure 7.5: Peak deformation amplitudes with an example of a regression line for consolidation calculation in PLAXIS on loose sand.

prominent in the results from PLAXIS simulations. This is probably because the PLAXIS model not manages to capture the big difference in tension and compression response very well. However, table 6.4 shows that displacements are lager in tension compared to compression for all simulations.

As can be seen in figure 6.9 to 6.12, the PLAXIS simulations manage to a larger extent to estimate a difference between compression and tension in packet 3 for total stress and pore pressure, at least compared to the displacement calculations. However, figure 6.14 shows that the total stress and pore pressure are greatly overestimated compared to the centrifuge experiments. Reasons for differences in PLAXIS simulations and centrifuge experiments are discussed in section 7.3.

7.2 Type of Behaviour and Material

This section presents a discussion on different behaviours for different parts of the soil around the suction caisson. The choice of materials in the simulations with respect to the soil behaviour, loosening of the sand, material model and friction angle, is also discussed.

7.2.1 Drained and Undrained Behaviour

During cyclic loading, the soil behaviour is primarily undrained. Results from centrifuge experiments in figure 6.6 and 6.7 and PLAXIS simulations in table 6.4 show that the total pressure and pore pressure measured at the lid invert is very similar. This indicates a close to undrained behaviour, at least at the top of the soil plug. However, the drainage is assumed to increase further down the soil plug and skirt. In that case, the displacements will in principal increase with permeability or lower pore fluid viscosity. At the skirt tip the behaviour is assumed to be close to fully drained. Comparison of the pore pressure in table 6.4 for undrained and consolidation calculations, shows only small differences. This is assumed to be due to the permeability in the consolidation calculation type, which probably is too small to account sufficiently for the consolidation effects. The behaviour of the soil in the consolidation simulations is therefore assumed to be close to undrained.

Simulations in PLAXIS are conducted using consolidation calculations, in addition to the two uttermost extents, undrained and drained calculations. Although the displacement of the caisson in principal increases with permeability, table 6.4 shows that drained calculations not always result in the largest displacements. When a load is applied in a drained simulation, the effective stress, and thus the soil stiffness and strength, is increased. In an undrained simulation, the stiffness and strength increase because of dilatancy, in addition to increased effective stresses. The premises for stiffness and strength in PLAXIS are therefore different in drained and undrained calculations. Consequently, there is not always easy to predict what type of calculation which will give the largest strains. The different calculation types in PLAXIS is in this study primarily used to get a deeper understanding of how the PLAXIS simulations work.

7.2.2 Materials

Calibration of Materials

In section 5.2.1 adaption of materials to match results from different soil tests is presented. In order to limit the required number of input parameters in PLAXIS, and thus maintain a simple and easy to understand model, all features of a soil cannot be included in one material. The materials will therefore have different stiffness parameters, and thus behave differently when applied to cyclic loading. The most suitable material for the recalculation of the centrifuge test is the one that describes the behaviour of the soil most precisely.

The stiffest behaviour is found in materials from the undrained tests. Parameters from undrained triaxial compression test is considered be most suitable to recreate the assumed undrained behaviour right below the caisson lid when pushed down. The material based the undrained triaxial extension test is assumed to best describe the opposite load direction, when the caisson is pulled up. The assumed drained behaviour around the skirt tip is expected to be best represented by the drained triaxial compression test material and the oedometer test material. The materials from drained tests are softer compared to undrained tests.

Note that the tests used for calibration of the materials are for monotonic loading. The behaviour is different for cyclic loading. However, the monotonic tests are the closest to actual soil behaviour examined in this study.

The parameters from the oedometer test are used to represent a best estimate material. The main reason for choosing this material is that the close to drained behaviour around the skirt tip is regarded as decisive for the caisson behaviour. In addition, the oedometer test is the only test where unloading and reloading is included. The stiffness parameters from the oedometer test is therefore preferred to the drained triaxial compression test.

Different Materials for Different Parts of the Model

A possibility in such calculations is to use different materials for different parts of the model. In order to capture the characteristic behaviour around the soil tip, a drained material can be

added around the soil tip, while the rest of the material is kept undrained. However, as the results illustrate, even the softest material from drained laboratory experiments demonstrates a far too stiff behaviour compared to the centrifuge experiments. To include the undrained and stiff material would therefore cause the simulations to differ more from the centrifuge experiments.

Loosening of Soil due to Installation

As the installation of the suction caisson is extremely hard, maybe even impossible, to recreate in PLAXIS, it is not included in the simulations. During installation a loosing of the sand around the skirt tip and skirt walls is inevitable. As the soil tests which are used to estimate stiffness parameters are conducted in extremely dense sand, the loosening of the soil is not accounted for when choosing a best estimate material. Looser materials, which parameters are given in table 5.3, are therefore used to approach this soft behaviour. However, the permeability is not adjusted for these materials, and the low permeability adapted to the very dense sand are used for all materials. The loosening and permeability of the soil is further discussed in section 7.3.

The Hardening Soil Model with Small Strain Stiffness

As described in section 5.2.2 the soil stiffness for very small strains is non-linearly dependent on strain amplitude. For the small loads and displacements in packet 1, the strains are in the range of very small strain stiffness, and this could be properly taken into account by using the Hardening Soil model with small strain stiffness. However, this material model will in the majority of the simulations result in a stiffer behaviour. As the soil displacements in the PLAXIS simulations in general are underestimated, the Hardening Soil model with small-strain stiffness would lead to the opposite of desired behaviour, smaller strains. The material model for Hardening Soil with small strain stiffness is therefore not further examined. However, in combination with looser sand and higher permeability, the soil model could have given a more realistic response.

Friction Angle

For calculations in PLAXIS, the peak friction angle, ϕ'_p, is used as input parameter, and not the ultimate value friction angle, ϕ'_{cv}. This will result in a stiffer behaviour. The friction angle has an impact on the displacements for sands that are currently experiencing its highest stress level. However, for the largest amplitudes the friction in the caisson skirt may during unloading and reloading be mobilised, and this is dependent on the friction angle. Hence, the displacements during repeated loading may therefore be affected by the difference in peak and ultimate frictional angle, especially for the load packets with largest amplitude. The concept of peak and ultimate value friction angle is presented in section 4.3.

7.2.3 Time Histories and Phase Changes

Figure 6.2 and 6.3 show the time history displacement curves, and figure 6.6 and 6.7 present the total stress and pore pressure against time. The curves for packet 1 and 2 are in general jagged. There may consequently be challenging to capture the small step changes of the response for these packets with small load amplitudes. There is therefore important to handle the results from these load packets with caution.

Figure 7.6 presents the displacement curves together with the applied load from packet 3. The most remarkable feature in this figure is the difference response for loads in tension and compression. The displacement curve in compression, upper side of the curve, has a more rounded path. This may indicate that the forces are transferred differently from the caisson to the soil in compression compared to tension. A bigger part of the forces may be transferred to the soil tip in compression.

Another notable observation in figure 7.6 is the phase difference between applied load and displacement response. As illustrated in figure 7.7 the phase difference is not present in the total and pore pressure curves. The pressures right below the caisson lid, should indeed follow the applied load. However, the pore pressure is in general also dependent on pore fluid flow further down the soil. The pore pressure response at lower levels is not necessarily in phase with the applied load. As the displacement not only is dependent on the soil behaviour at the cais-

son lid, but in the entire soil, its response can be out of phase. The phase difference may be an indication of existence of pore fluid flow and a dependency of displacement response on this flow.

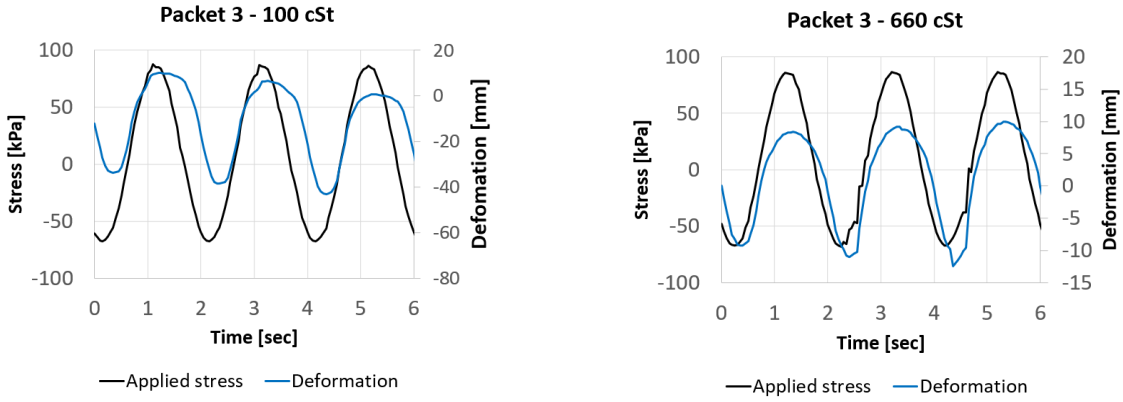

Figure 7.6: Applied stress together with displacement response. The curves illustrate a phase difference.

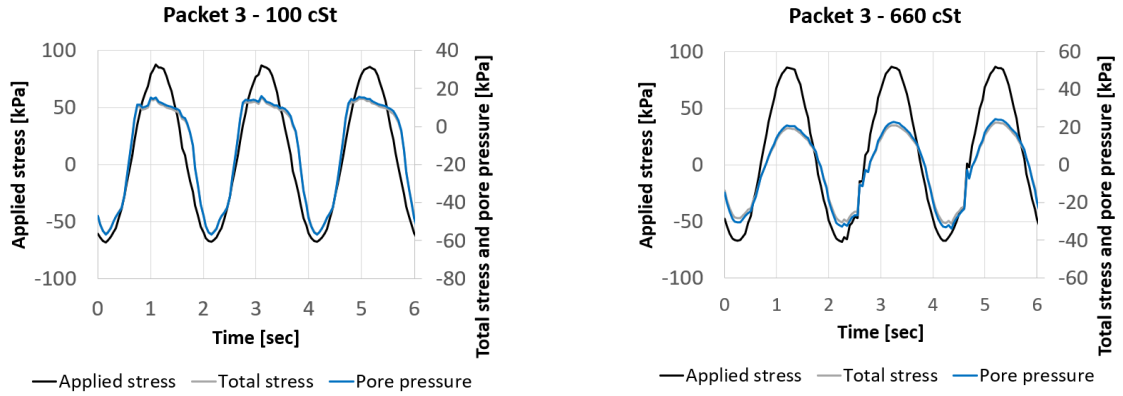

Figure 7.7: Applied stress together with total stress and pore pressure response.

7.3 Reasons for Differences in Centrifuge Experiments and PLAXIS Simulations

In this section possible reasons for difference in caisson response in centrifuge experiments and PLAXIS simulations, including loosening of the soil due to installation, consolidations and redistribution of forces, a gap between caisson lid and soil, and air bubbles in the pore fluid is discussed.

7.3.1 Loosening of Soil Due to Installation

The installation process causes the sand to loosen around the caisson. The published information on this topic is limited, however a reasonable assumption is that the soil around the skirt tip will be greatly affected by the installation process.

Table 6.5 shows displacements from simulations where the best estimate material is replaced by the loose material at the skirt tip. The soil is exposed to load packet 2, and a consolidation calculation is performed. A small increase in displacement response is observed. However, the increase is very small compared to the simulations where the whole soil cluster is replaced by the loose material. This may indicate that not only the soil around the skirt tip is affected by the installation, but also soil around the skirt walls. The size of the possibly loosened area is however unknown. A more detailed study of the installation process and its effect on the loosening of the soil is therefore necessary in order to give a good estimate of the size and features of the loosened area.

7.3.2 Consolidation and Redistribution of Forces

The permeability, k, is in these simulations a parameter associated with uncertainties. Even though theoretical values are presented in section 5.2.4 based on soil test values introduced in section 4.3, the values should be handled with caution.

Table 6.6 presents how the displacement, total stress and pore pressure are dependent on the permeability for consolidation analyses of loose sand exposed to load packet 2. The table shows that the permeability which approaches drained behaviour is many times higher than the initial permeability of 8.04×10^{-3} m/s in prototype scale. The permeability has to increase to $k = 8.04 \times 10^{2}$ only to reach the displacement values of 5.07 mm which is found in the centrifuge experiments for the similar load packet. This indicates that the permeability parameter has to be carefully calibrated to match the actual values in the centrifuge experiments. The loosening of the sand due to installation is not taken into account when the permeability is estimated. In this way recalculation cannot be done with a precise parameter for permeability.

Figure 4.6 in section 4.3 illustrates normalised pore pressure dissipation time histories which can be used to calibrate the permeability parameter, k. However, there are no available information on absolute values of the pore pressure and on how the normalisation is done, which makes it very hard to recreate the experiment. In addition, these types of tests for suction caisson are highly dependent on redistribution of forces from soil plug to caisson skirt.

The total applied load will in general not necessarily reach down to the skirt tip since parts of the load may be taken up as friction along the skirt. This redistribution of forces can be numerically controlled by stiffness parameters in the soil plug, skirt walls and the soil along the skirt. In cases where the soil along the skirt is stiff, e.g. low mobilised, a big part of the forces will be redistributed during the consolidation process, and a smaller part of the forces will contribute to squeeze the soil plug together. Pore water in the soil will immediately after the change in load step carry all the load due to its high stiffness. As the consolidations process starts, the magnitude of the load which is transferred to the softer soil grains or to the skirt walls, is depending on the stiffness of the soil along the skirt and the permeability of the soil.

If no redistribution of forces were present, the total stress in an arbitrary location below the suction caisson would not change after pore pressure dissipation, i.e. all stresses would transform into effective stresses. However, observations show that this is not the case in general. Figure 7.8 illustrates how the total stress, σ, and effective stress, σ', change with time as pore pressure dissipate at a point right below the caisson lid.

During pore pressure dissipation, the reduction of the total stress is 20 kPa. This reduction in the total stress represents the stress transferred to the skirt wall. In addition, the effective stress increases with roughly 10 kPa. Consequently, the pore pressure will reduce with 30 kPa. Notice that the change in pore pressure is the sum of change in effective stress and total pressure. The pore pressure change is therefore not only dependent on how fast pore fluid dissipates, but also on the amount of load that is transferred to the skirt walls. Hence, the permeability cannot be determined by simply measuring the pore pressure stresses following a load step change without accurate knowledge of the stiffness of the system.

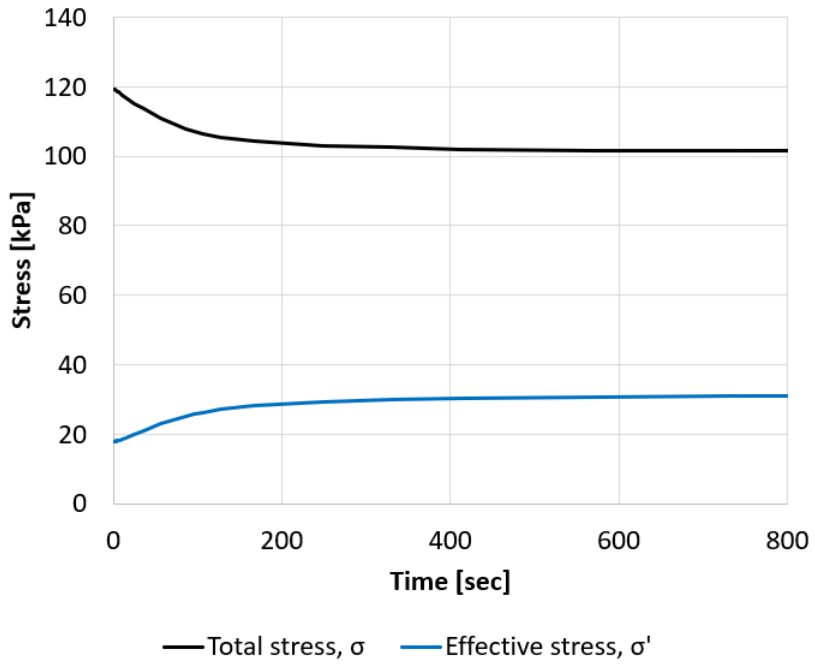

Figure 7.8: The figure illustrates how effective and total stresses change in a PLAXIS simulation during consolidation due to redistribution of stresses and pore water dissipation. The values are taken from a point right below the caisson lid.

7.3.3 Gap Between Caisson Lid and Soil

When the caisson is installed, a gap between the caisson lid and soil may occur. This is in many cases hard to avoid, especially if suction is the only mechanism used to penetrate the caisson. During compression the lid can be in contact with the soil, but for tension loading a pocket filled of water can be created. Consequently, the response will be softer in tension compared to compression. In addition, the water pocket may cause the response to be equal for total stress and pore pressure. Table 6.2 and 6.3 show that this is the case for the centrifuge tests. To account for this gap in the PLAXIS simulations, a thin area of softer can soil replace the original soil just below the caisson lid.

Table 6.7 shows that the displacements in the PLAXIS simulations increase as the thin soil layer beneath the caisson lid becomes softer. The simulations are done for a loose sand exposed to load packet 2. The displacements for the second softest material are 4.26 and 6.02 mm in compression and tension, respectively. This is very close to the displacements from the centrifuge

experiment with pore fluid viscosity 100 cSt which are 5.7 mm in compression and tension. The softer layer beneath the caisson lid can be studied in a combination with changes in permeability. A mix of these two elements may give response closer to the centrifuge experiments.

7.3.4 Air Bubbles in Pore Fluid

Another reason why the response in the simulations differ from the centrifuge experiments may be that the pore fluid contains air bubbles. The fluid is in general very stiff, however air bubbles make the fluid more compressible. In undrained triaxial tests a back pressure is applied to the soil sample to reduce the size of the air bubbles. The stiffness of the soil increases with the back pressure, but even with a very large pressure, there is hard to completely remove the air in the fluid. In an experiment like the centrifuge experiment, air bubbles may presumably be present in the pore fluid.

The air bubbles, and thus the soil, are assumed to be squeezed together when a cyclic compression load is applied. A bigger part of the forces may therefore be taken by the skirt tip, and consequently, the deformations will be larger compared to experiments with no air in the pore fluid. In addition, the total stress and pore pressure response may become smaller due the redistribution of forces, as more of the loads are taken by the skirt tip and less is transferred to the soil right beneath the caisson lid. As the simulations do not account for air bubbles in the pore fluid, the bubbles can explain both the underestimated deformation and the overestimated total stress and pore pressure response in the simulations.

Table 6.2 and 6.3 and figure 6.14 and 6.15 illustrate that the total stress and pore pressure increase with permeability for centrifuge experiments. This strange behaviour may be explained by air pockets in the pore fluid. A possibility is that the experiments with higher pore fluid viscosity contain more air than the experiments with lower viscosity.

Air bubbles in the pore water can be accounted for in PLAXIS by reducing the Bulk modulus of water, which will make the water softer. However, this is not further studied in this thesis. Note that for the total stress and pore pressure the initial values from the centrifuge experiments are unknown. This discussion is therefore solely based on cyclic peak amplitudes.

7.3.5 Summary of Reasons for Difference in Centrifuge Experiments and PLAXIS Simulations

In this section several reasons for different response in PLAXIS analyses and centrifuge experiments are introduced, in which some of the theories have been tested using PLAXIS simulations. Loosening of the soil material, calibration of permeability, gap between caisson lid and soil and air bubbles in the pore fluid are mentioned. All of these arguments will presumably result in larger displacements and behaviour closer to the centrifuge experiments. An assumption is therefore that a combination of several of the reasons given in this section will give the most accurate behaviour, and lead to results from PLAXIS analyses more equal to centrifuge experiments. This means that the whole gap between PLAXIS analyses and centrifuge tests does not need to be covered by one parameter or property only.

7.4 Relevance of Centrifuge Experiments and Use of Data from External Sources

A lot of elements need to be taken into account for experiments conducted in model scale, when trying to adapt the results to prototype scale. As for centrifuge experiments, the soil stresses are similar those of the prototype, which makes the adaption a bit easier. However, the use of smaller dimensions may be challenging in order to capture all the features of a prototype model precisely. The use of a 0.5 mm skirt wall thickness in the centrifuge test, may, for instance, introduce a scale effect as it changes the ratio between skirt wall thickness and grain size compared to prototype conditions.

The soil sample used during the centrifuge experiments are very dense, which is typical for North Sea sands. However, during installation parts of the soil around the suction caisson may become looser, and this should be taken into account. Soil parameters measured in very dense sand may therefore differ from what is actually present in the soil samples after installation.

The centrifuge experiment has used one single suction caisson to represent one of the caissons in a tripod foundation. Even though several types of loading sequences have been applied to the caisson, the interaction between the caissons, such as dependency on distance between them, cannot be estimated from the centrifuge experiments examined in this study.

The data from the centrifuge experiments are collected from sources at the UWA. As the experiments have been conducted by a third party, information about how the experiments have been carried out is limited to what is written and published. This leads to less knowledge of how successful or trustful the experiments and results are. By not having this information the risk of misinterpreting the results from the experiments increases.

Chapter 8

Conclusion and Recommendations for Further Work

8.1 Summary and Conclusion

This thesis has examined the response of offshore wind tribunes with respect to cyclic loading. Offshore installations are in general subject to cyclic loading due to wind, waves and currents. However, compared to traditional and heavy offshore installations in the oil and gas industry, offshore wind turbines are more susceptible to cyclic loading. Thus, the cyclic behaviour of sand is of key importance to this thesis.

The thesis is seen in light of the theory on cyclic response of suction caissons and the HCA model. During cyclic loading, a combination of average loads and a large number of small-strain cyclic loads will cause the soil to accumulate pore pressure or deformation, or both. The HCA model, described in this thesis, accounts for these effects by using an explicit calculation strategy which calculates the accumulation directly. Implicit calculation is performed in order to update the strain amplitude after a large number of cycles. The accumulation is given by six independent functions.

The UWA has conducted several centrifuge experiments on very dense Baskarp sand. The experiments aim to represent one of three suction caissons supporting an offshore wind turbine

in the North Sea. In order to make the experiments as realistic as possible the caisson is installed using suction. The installation is followed by cyclic loading, and the response of the caisson is investigated.

When it comes to the first objective of the thesis, the results examined from the centrifuge experiments performed at the UWA demonstrate a significant difference in response for compression and tension loading. This is in this master thesis discussed to be due to a softer behaviour in tension. Experiments with different pore fluid viscosity is conducted and the effect of drainage is investigated in the thesis. As the experiments with lowest pore fluid viscosity result in the largest displacements, the drainage is assumed to affect the results. An observed phase difference in the response support this assumption.

Regarding the second objective of the thesis, the recalculation of the centrifuge experiments illustrates the challenge of simulating the complex caisson behaviour. Even though material parameters calibrated from oedometer tests are assumed to best estimate the caisson response, simulations using a looser material are closest to recreate the response from the centrifuge experiments. However, even with a loose material, the displacements are in the simulations mainly underestimated, while the total stress and pore pressure are overestimated.

The different response in the centrifuge experiments compared to the simulations are assumed to be due to loosening of the sand during installation, limitations in calibration of the permeability parameter, redistribution of forces, water pocket beneath the caisson or air bubbles in the pore fluid. The difference may be caused by one single or a combination of the aforementioned reasons.

8.2 Recommendations for Further Work

Based on the thesis the following recommendations for further work are proposed.

Input parameters in the PLAXIS simulations are not based on proper sand specified cyclic laboratory tests. A more precise estimation of the parameters is recommended for further studies. The permeability is of special importance and a better system to calibrate this parameter should

be developed. A possibility is to measure the amount of dissipated pore fluid during installation or perform a steady state seepage analysis after installation.

It would also be advantageous to perform a more idealised test to calibrate interface friction between the sand and aluminium caisson. A pull-out test of a simple aluminium plate will result in interface parameters that are not so heavily dependent on initial stresses as the extraction resistance tests performed in connection with the centrifuge experiments. To calibrate the effect of loosening of sand due to the installation process, a reference test where the caisson is installed in loose can be performed. Comparison of results from experiments with dense sand will give an indication of the extent of the loosened area.

The installation of the caisson in the centrifuge experiments is performed by suction only. Consequently, there is a major risk of existence of a water pocket beneath the caisson lid. Further experiments should avoid this problem either by covering the pocket with fill dirt, which is often done in practice, or by pushing the caisson into the seabed instead of just pulling.

For further analyses in PLAXIS or other simulation programs the initial value of the total stress and pore pressure should be known. This is useful to make sure the response of the simulations matches the centrifuge experiments. In addition, simulations using a lower Bulk modulus for water to investigate the hypothesis of air bubbles in the water would be of great interest.

The accumulated effects due to cyclic loads are very important for suction caissons supporting offshore wind turbines. It will be highly interesting to study these effects in a computer simulation software, such as PLAXIS. At NGI, the HCA model is already implemented into PLAXIS. Recalculation of the centrifuge experiments by the use of this model will be of great value, especially as the long-term effects of cyclic loads can be predicted in this model.

List of Figures

List of Tables

Bibliography

Andersen, K. H. (1989). Bearing capacity of gravity platform foundations on sand - static and cyclic laboratory test in very dense sand.

Andersen, K. H. (2009). Bearing capacity under cyclic loading—offshore, along the coast, and on land. the 21st bjerrum lecture presented in oslo, 23 november 2007. *Canadian Geotechnical Journal*, 46(5):513–535.

Andersen, K. H. and Berre, T. (1999). Behaviour of a dense sand under monotonic and cyclic loading comportement d'un sable dense sous chargement monotonique et cyclique.

Andersen, K. H. and Jostad, H. P. (1999). Skirted offshore foundations and anchors in sand.

Andersen, K. H., Jostad, H. P., and Dyvik, R. (2008). Penetration resistance of offshore skirted foundations and anchors in dense sand. *Journal of geotechnical and geoenvironmental engineering*, 134(1):106–116.

Andersen, K. H. and Schjetne, K. (2012). Database of friction angles of sand and consolidation characteristics of sand, silt, and clay. *Journal of Geotechnical and Geoenvironmental Engineering*, 139(7):1140–1155.

Bienen, B., Klinkvort, R., O'Loughlin, C., Zhu, F., and Byrne, B. (2018a). Suction caissons in dense sand, part ii: vertical cyclic loading into tension. *Géotechnique*, pages 1–15.

Bienen, B., Klinkvort, R. T., O'Loughlin, C., Zhu, F., and Byrne, B. (2018b). Suction caissons in dense sand, part i: installation, limiting capacity and drainage. *Géotechnique*, pages 1–16.

Blaker, O., Lunne, T., Vestgården, T., Krogh, L., Thomsen, N., Powell, J., and Wallace, C. (2015). Method dependency for determining maximum and minimum dry unit weights of sands. pages 1159–1166.

Brinkgreve, R., Kumarswamy, S., and Swolfs, W. (2017). Plaxis 2d manual, 2d material models manual 2017.

Bybee, K. et al. (2001). Hoover-diana deepwater drilling and completions. *Journal of petroleum technology*, 53(07):33–35.

Bye, A., Erbrich, C., Rognlien, B., Tjelta, T., et al. (1995). Geotechnical design of bucket foundations. In *Offshore Technology Conference*. Offshore Technology Conference.

Houlsby, G. (2016). Interactions in offshore foundation design. *Géotechnique*, 66(10):791–825.

Houlsby, G. and Byrne, B. (2004). Calculation procedures for installation of suction caissons. *Report No. OUEL2268/04, University of Oxford*.

Ibsen, L. B. (2008). Implementation of a new foundations concept for offshore wind farms. In *Nordisk Geoteknikermøte*, pages 19–33. Norsk Geoteknisk Forening.

Jia, J. (2018). Suction piles/caissons. In *Soil Dynamics and Foundation Modeling*, pages 655–668. Springer.

Mackereth, F. (1958). A portable core sampler for lake deposits. *Limnology and oceanography*, 3(2):181–191.

Niemunis, A., Wichtmann, T., and Triantafyllidis, T. (2005). A high-cycle accumulation model for sand. *Computers and geotechnics*, 32(4):245–263.

Peire, K., Nonneman, H., and Bosschem, E. (2009). Gravity base foundations for the thornton bank offshore wind farm. *Terra et Aqua*, 115:19–29.

Terzaghi, K. (1951). *Theoretical soil mechanics*, pages 265–296. Chapman And Hall, Limited.; London.

Tjelta, T. (2015). The suction foundation technology. *Frontiers in Offshore Geotechnics III*, 85.

Tjelta, T., Aas, P., Hermstad, J., Andenaes, E., et al. (1990). The skirt piled gullfaks c platform installation. In *Offshore Technology Conference*. Offshore Technology Conference.

Wichtmann, T. (2005). *Explicit accumulation model for non-cohesive soils under cyclic loading*. PhD thesis, Inst. für Grundbau und Bodenmechanik Bochum University, Germany.

Wichtmann, T., Niemunis, A., and Triantafyllidis, T. (2010). On the "elastic" stiffness in a high-cycle accumulation model for sand: a comparison of drained and undrained cyclic triaxial tests. *Canadian Geotechnical Journal*, 47(7):791–805.

Zhou, Y.-g. and Chen, Y.-m. (2005). Influence of seismic cyclic loading history on small strain shear modulus of saturated sands. *Soil Dynamics and Earthquake Engineering*, 25(5):341–353.